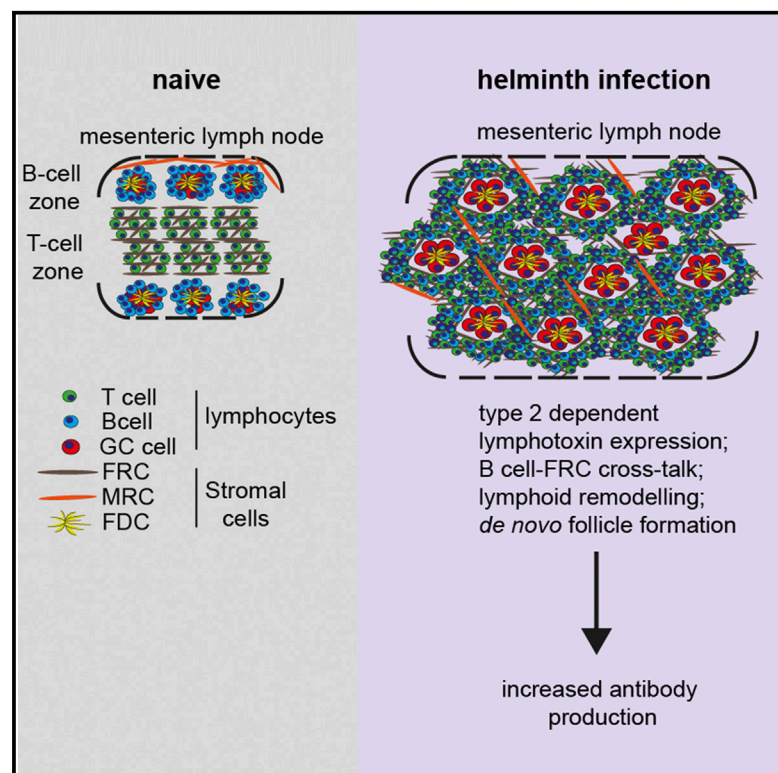


## Lymphotoxin-Dependent B Cell-FRC Crosstalk Promotes De Novo Follicle Formation and Antibody Production following Intestinal Helminth Infection

### Graphical Abstract



### Authors

Lalit Kumar Dubey, Luc Lebon, Ilaria Mosconi, ..., Burkhard Ludewig, Sanjiv A. Luther, Nicola L. Harris

### Correspondence

nicola.harris@epfl.ch

### In Brief

Intestinal helminth infection drives type 2 immune responses in the draining mLN. Dubey et al. demonstrate in mice that type 2 inflammation drives lymphoid remodeling resulting from lymphotoxin-dependent crosstalk between B cells and FRCs. Such crosstalk promotes *de novo* follicle formation and supports the production of parasite-specific antibodies.

### Highlights

- Helminth infection drives *de novo* B cell follicle formation in the draining mLN
- B cells promote FRC proliferation and activation via lymphotoxin-LT $\beta$ R signaling
- IL-4R $\alpha$  is necessary for helminth-induced lymphotoxin expression by B cells
- LT $\beta$ R signaling to FRCs promotes *de novo* follicle formation and antibody production



# Lymphotoxin-Dependent B Cell-FRC Crosstalk Promotes De Novo Follicle Formation and Antibody Production following Intestinal Helminth Infection

Lalit Kumar Dubey,<sup>1</sup> Luc Lebon,<sup>1</sup> Ilaria Mosconi,<sup>1</sup> Chen-Ying Yang,<sup>3</sup> Elke Scandella,<sup>2</sup> Burkhard Ludewig,<sup>2</sup> Sanjiv A. Luther,<sup>3</sup> and Nicola L. Harris<sup>1,\*</sup>

<sup>1</sup>Global Health Institute, School of Life Sciences, École Polytechnique Fédérale de Lausanne (EPFL), station 19, 1015 Lausanne, Switzerland

<sup>2</sup>Institute of Immunobiology, Kantonsspital St. Gallen, 9007 St. Gallen, Switzerland

<sup>3</sup>Department of Biochemistry, Center for Immunity and Infection Lausanne, University of Lausanne, 1066 Épalinges, Switzerland

\*Correspondence: [nicola.harris@epfl.ch](mailto:nicola.harris@epfl.ch)

<http://dx.doi.org/10.1016/j.celrep.2016.04.023>

## SUMMARY

Secondary lymphoid tissues provide specialized niches for the initiation of adaptive immune responses and undergo a remarkable expansion in response to inflammatory stimuli. Although the formation of B cell follicles was previously thought to be restricted to the postnatal period, we observed that the draining mesenteric lymph nodes (mLN) of helminth-infected mice form an extensive number of new, centrally located, B cell follicles in response to IL-4R $\alpha$ -dependent inflammation. IL-4R $\alpha$  signaling promoted LT $\alpha_1\beta_2$  (lymphotoxin) expression by B cells, which then interacted with CCL19 positive stromal cells to promote lymphoid enlargement and the formation of germinal center containing B cell follicles. Importantly, de novo follicle formation functioned to promote both total and parasite-specific antibody production. These data reveal a role for type 2 inflammation in promoting stromal cell remodeling and de novo follicle formation by promoting B cell-stromal cell crosstalk.

## INTRODUCTION

Secondary lymphoid tissues exhibit a highly organized structure characterized by a central T cell zone and a periphery in which B cell follicles are in close contact with the subcapsular sinus (SCS) (Mueller and Germain, 2009). Stromal cells play multiple roles in lymphoid tissues, acting as structural cells in addition to secreting chemokines that direct T and B cells to their respective territories. The B cell zone contains CD35 positive follicular dendritic cells (FDCs), which trap immune-complexed antigens, promote B cell migration and clear apoptotic B cells from the germinal center (Heesters et al., 2014). The T cell zone harbors a rich network of podoplanin (Pdpn) positive fibroblastic reticular cells (FRCs), which provide a scaffold along which recirculating T and B cells migrate and secrete extracellular matrix proteins to form conduits that transport small lymph borne antigens from

the SCS to the underlying B cell follicles and T cell zone (Bajénoff and Germain, 2009; Roozendaal et al., 2009; Sixt et al., 2005). FRCs also coordinate the interaction of T cells and dendritic cells (DCs) by virtue of their expression of the chemokines CCL19 and CCL21 (Siegert and Luther, 2012) and regulate T cell homeostasis and tolerance through the production of the survival factor interleukin-7 (IL-7) (Link et al., 2007) and the expression of major histocompatibility complex (MHC) proteins (Fletcher et al., 2010). More recently, FRCs were shown to regulate T cell expansion via the secretion of the soluble mediator, nitric oxide, and to support B cell survival through the secretion of B-cell activating factor (Cremasco et al., 2014; Siegert and Luther, 2012).

The initiation of adaptive immune responses involves lymphoid swelling resulting from the rapid trapping of naive T and B cells in response to inflammatory stimuli (Yang et al., 2014). FRCs are known to expand (Acton et al., 2014; Astarita et al., 2015; Yang et al., 2014) and to proliferate in response to inflammation, and the proliferation phase involves the delivery of LT $\beta$ R signals to the stromal cells by incoming T and B cells (Yang et al., 2014). The activation and expansion of FRCs has been reported to be necessary for the generation of protective anti-viral immunity (Chai et al., 2013; Cremasco et al., 2014); however, their impact on host immunity against pathogens that elicit type 2 inflammation remains unknown.

Intestinal helminths represent a major global health problem, infecting approximately 2 billion people worldwide, with children harboring the largest worm burdens. These parasites typically elicit type 2 inflammation and often form chronic infections (Bethony et al., 2006). The natural murine helminth, *Heligmosomoides polygyrus bakeri* (*Hpb*), serves as an excellent laboratory tool for the evaluation of host-helminth interactions and has been used extensively to broaden our understanding of protective immunity against these organisms (Harris, 2011). Primary infection leads to chronic infection in susceptible C57BL/6J mice; however, the adult worms are eventually expelled from the intestine by a process that requires CD4<sup>+</sup> T cells and type 2 immunity (Mohrs et al., 2001). Thereafter, mice are resistant to repeated infections, with helminth-specific antibodies playing a crucial role in this process (McCoy et al., 2008; Wojciechowski et al., 2009).

In the current study, we used flow cytometry and whole-slide scanning along with confocal analysis of cryosections to

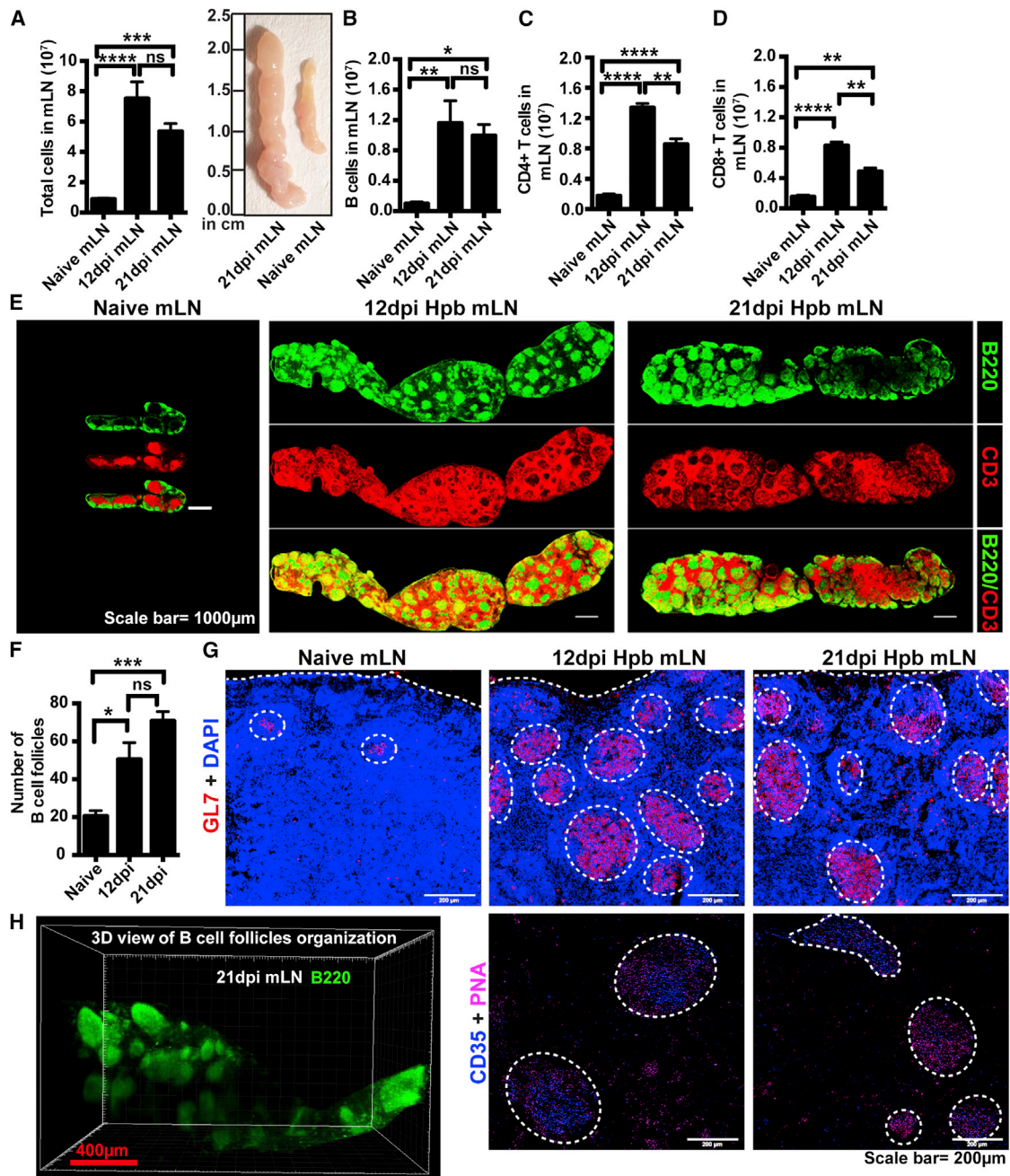


### Figure 1. *Hpb* Infection Triggers mLN Swelling and De Novo B Cell Follicle Formation

C57BL/6J mice were infected with *Hpb*, and the entire chain of the mLN was collected at 0 (naive), 12, and 21 dpi.

(A) Total cellularity and size of the mLN from naive or infected mice; data represent mean  $\pm$  SEM, pooled from three independent experiments with  $n \geq 3$  mice per group.

(B–D) Total number of B cells (B), CD4<sup>+</sup> T cells (C), and CD8<sup>+</sup> T cells (D) in mLN as determined by flow cytometry. Data represent mean  $\pm$  SEM from one experiment and are representative of two independent experiments with  $n \geq 3$ –4 mice per group.

(E) Whole-length mLN cryosections showing single and combined staining of B cells (green, B220<sup>+</sup>) and T cells (red, CD3<sup>+</sup>) in naive or infected mice. Scale bar, 1,000  $\mu$ m.

(F) Numbers of B cell follicles (B220<sup>+</sup>) were counted on a graphic tablet at higher magnification; data represent mean  $\pm$  SEM pooled from two independent experiments ( $n = 4$  mLN/time point).

(G) mLN cryosections showing combined staining for germinal center B cells (red, GL7<sup>+</sup>) and nuclei (DAPI; blue), or combined overlay staining for germinal center B cells (magenta, PNA<sup>+</sup>) and FDCs (blue, CD35<sup>+</sup>) in naive or infected mice. Scale bar, 200  $\mu$ m.

(legend continued on next page)

visualize the structural organization and function of the hematopoietic and non-hematopoietic (stromal) compartments of the draining mesenteric lymph node (mLN) following chronic *Hpb* infection. We observed a profound remodeling of the mLN, including the de novo formation of centrally located, germinal center containing, B cell follicles, and the remodeling and proliferation of FRCs. IL-4R $\alpha$  signaling lead to the indirect activation of CCL19 positive stromal cells by promoting the upregulation of lymphotoxin expression on B cells and thereby promoting B cell-stromal cell crosstalk. B cell-stromal cell crosstalk was necessary for de novo follicle formation and functioned to promote antibody production in response to the invading helminth.

## RESULTS

### Intestinal Helminth Infection Results in a Dramatic Swelling of the mLN and the Formation of New B Cell Follicles

We have previously reported that the mLN, which drains directly from the small intestine, forms the primary site for the generation of inflammatory type 2 immune responses following *Hpb* infection, with inflammation peaking between days 10 and 14 following infection and slowly diminishing thereafter (Mosconi et al., 2015). In keeping with these data, we found that *Hpb* infection resulted in a profound increase in the size and cellularity of the mLN (Figure 1A), including increased numbers of B cells (Figure 1B), CD4<sup>+</sup> T cells (Figure 1C), and to a lesser extent CD8<sup>+</sup> T cells (Figure 1D). Although the numbers of B cells remained unchanged from 12 to 21 days post-infection (dpi), the number of T cells significantly decreased during this period with B cells therefore representing the dominant lymphocyte population at later time points. Staining of cryosections with antibodies specific for B220 (green panel) and CD3 (red panel) revealed an expected microarchitecture in naive mice with B cell follicles located at the periphery of the mLN, and a central paracortical region rich in T cells (Figure 1E, left panel). *Hpb* infection resulted in a dramatic alteration of lymphoid structure characterized by a profound increase in the number of B cell follicles and the reorganization of T cell zones to tightly encompass these newly formed follicles (Figures 1E, middle and right panels, and 1F). Infection also resulted in an increase in the number and size of follicles containing germinal center B cells (PNA<sup>+</sup> or GL7<sup>+</sup>) and FDCs (CD35<sup>+</sup> or FDC-M1<sup>+</sup>) (Figures 1G, S1A, and S1B). To further substantiate our histological findings that new B cell follicles formed within the T cell-rich central region of the mLN, we imaged thick sections (up to 500  $\mu$ m) taken from the center of the node and subjected to optical clearing (Ke et al., 2013) (Figure S1C). Imaging using light sheet microscopy clearly showed the presence of B cell follicles deep within the mLN (Figure 1H; Movie S1). Together these data demonstrate that chronic *Hpb* infection results in dramatic changes to mLN organization, including the de novo formation of centrally located B cell follicles.

### Infection-Induced Swelling of the mLN Is Accompanied by Stromal Cell Proliferation and Re-organization

We next asked whether the observed changes in hematopoietic compartments were accompanied by corresponding alterations in stromal cell subsets. Fluorescence-activated cell sorting (FACS) analysis revealed a significant increase in total CD45 negative (CD45<sup>-</sup>) stromal cells of  $\geq 4$ -fold at 12 and 21 dpi (Figure 2A), which was comparable to the  $\geq 5$ -fold increase in lymphocyte numbers seen at these time points (Figures 1B–1D). This included significant increases in Pdpn<sup>+</sup>CD31<sup>-</sup> FRCs, Pdpn<sup>+</sup>CD31<sup>+</sup> lymphatic endothelial cells (LECs), Pdpn<sup>-</sup>CD31<sup>+</sup> blood endothelial cells (BECs), and Pdpn<sup>-</sup>CD31<sup>-</sup> double-negative (DN) cells (thought to include FRC precursors) (Chai et al., 2013) (Figures 2B–2E and S2A). Pdpn<sup>+</sup>CD31<sup>-</sup> FRCs made up the majority of the stromal cell population in infected mice, with proliferation likely contributing to their expansion as an increased proportion of these cells expressed Ki-67 in infected mice (Figure 2F).

Histological analysis of serial mLN sections revealed the presence of a FRC network (identified as Pdpn, CD140 $\alpha$  [also known as PDGFR- $\alpha$ ], ER-TR7, and laminin positive cells) (Link et al., 2007), which formed an interconnected structure in the T cell-rich area of both naive and infected mice, and which surrounded the newly formed B cell follicles in infected mice (Figure 2G). The total area of the mLN occupied by FRCs significantly increased following *Hpb* infection (Figure S2B). We further confirmed stromal cell remodeling around the newly formed central B cell follicles by imaging thick mLN sections of tissue taken from the center of the node. 3D reconstruction using IMARIS confirmed the reorganization of stromal network (positive for ER-TR7<sup>+</sup>) around B cell follicles (Figures 2H and S2C; Movies S2 and S3). In contrast to the mLN, Peyer's patches from infected mice exhibited an overall enlargement in cellularity but no organizational alterations in either the hematopoietic or stromal cell compartments (Figure S2D).

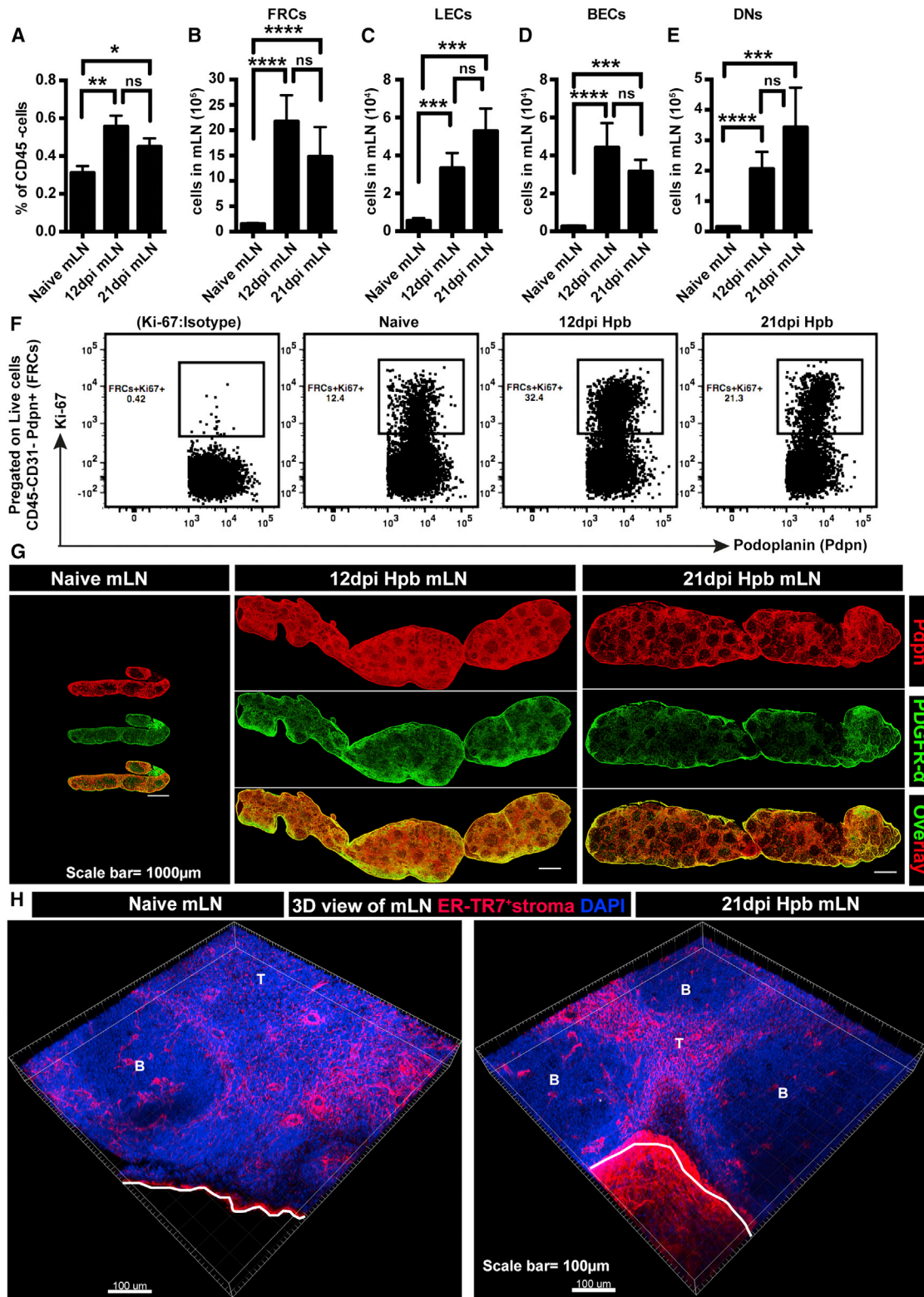
Closer analysis of the Pdpn<sup>+</sup> laminin<sup>+</sup> FRC network of the draining mLN revealed the presence of a ridge around the mantle of newly formed B cell follicles, which tightly surrounded the germinal center (GL7<sup>+</sup>) B cells and supported interactions between naive B cells (immunoglobulin D<sup>+</sup> [IgD<sup>+</sup>]) and T cells (CD3<sup>+</sup>) (Figures 3A, 3B, and S3A). Higher magnification visualization revealed that FRCs formed intimate contacts with both naive B cells and T cells within this region (Figure S3B). We could also detect T cells within the germinal center (Figures 3A and 3B), most likely represented by the previously described IL-4-producing T follicular helper cells (T<sub>FH</sub>) known to be expanded in response to *Hpb* infection (King and Mohrs, 2009).

FRCs contain both T cell zone fibroblastic reticular cells and marginal zone reticular cells (MRCs) (Yang et al., 2014). The latter are normally located in the SCS and can be identified by their selective expression of podoplanin, MadCAM-1, and RANKL (Cremasco et al., 2014; Katakai et al., 2008; Yang et al., 2014). B cell follicle development is known to require the presence of

For (E) and (G), images are representative of three or more experiments with at least two to three mice/group/time point.

(H) 3D view of mLN showing B cell follicle organization (B220<sup>+</sup> cells). Images are representative of two independent experiments. \* $p < 0.05$ , \*\* $p < 0.01$ , \*\*\* $p < 0.001$ , and \*\*\*\* $p < 0.0001$  (ANOVA, Bonferroni's multiple comparison test).

See also Figure S1 and Movie S1.



(legend on next page)

CXCL13-producing FDCs (Wang et al., 2011), and Jarjour et al. (2014) recently described that FDCs can arise from the clonal expansion and differentiation of MRCs, which are also capable of producing CXCL13 (Katakai et al., 2008). Analysis of these cells in our experiments revealed that in the naive state MRCs (identified as Pdpn<sup>+</sup>MadCAM1<sup>+</sup>RANKL<sup>+</sup>) can be found below the SCS region but not in the paracortical region of the mLN (Figure S3C). During *Hpb* infection, MRCs expanded and migrated away from the SCS to enter the central regions of the mLN (Figure 3C, boxes 2–4). This migration of MRCs away from the SCS coincided with the de novo formation of FDC-containing B cell follicles within the same region (Figures 1E and 1G). In light of the findings of Jarjour et al. (2014), our observations raise the intriguing possibility that MRC migration into the central regions of the mLN contributes to the de novo formation of centrally located follicles. Taken together, these indicate that helminth infection drives profound stromal cell remodeling in the mLN including MRC migration and the expansion and re-organization of FRCs to surround newly formed and centrally located B cell follicles.

#### IL-4R $\alpha$ Is Required for mLN Swelling and Remodeling following Intestinal Helminth Infection

IL-4 receptor alpha (IL-4R $\alpha$ ) signaling via IL-4 and IL-13 serves as a prime nexus point in driving protective type 2 immunity following *Hpb* infection (Finkelman et al., 2004; Urban et al., 1998), prompting us to examine the impact of this pathway on the observed changes to mLN organization. Naive IL-4R $\alpha$  knockout (IL-4R $\alpha$ <sup>-/-</sup>) mice exhibited normal mLN weight, cellularity, and central T cell zone versus peripheral B cell zone organization (Figures 4A–4D). In response to infection the mLN of IL-4R $\alpha$ <sup>-/-</sup> animals exhibited slight increases in weight and cellularity, although this was decreased as compared to wild-type mice (Figures 4A–4C and S4A). IL-4R $\alpha$ <sup>-/-</sup> animals also failed to reorganize the T cell compartment, and, although B cell follicles present in naive IL-4R $\alpha$ <sup>-/-</sup> animals contained FDCs, these mice failed to generate new FDC-containing B cell follicles in central region of the mLN, or to produce increased amounts of CXCL13 (Figures 4D and S4B–S4D). Furthermore, IL-4R $\alpha$ <sup>-/-</sup> mice had reduced level of total and parasite-specific IgG1 (Figures S4E and S4F) and IgE (Figures S4G and S4H) antibodies in response to infection. FRC networks in IL-4R $\alpha$ <sup>-/-</sup> mice looked normal under naive conditions; however, these mice failed to exhibit the expected increase in FRC density following infection (Figures 5A and 5B), correlating

with a decrease in the total number and proliferation of these cells (Figures 5C and 5D). These data unveil a previously unidentified role for IL-4R $\alpha$  signaling in promoting stromal cell expansion and lymphoid re-organization.

To examine the possible mechanism(s) by which IL-4R $\alpha$  signaling promotes stromal cell expansion and de novo follicle formation, we investigated which cells expressed this receptor. As expected, IL-4R $\alpha$  expression was clearly detectable on the surface of hematopoietic cells and increased significantly following infection (Figures S5A and S5B). By contrast, only a very small proportion of mLN stromal cells expressed IL-4R $\alpha$ , with no expression on FRCs (Figure S5A).

FRC proliferation is known to be promoted by lymphotoxin-expressing hematopoietic cells (Lu and Browning, 2014; Yang et al., 2014), and it has been previously reported that *Hpb* infection increases lymphotoxin expression on lymphocytes (León et al., 2012). We therefore investigated whether IL-4R $\alpha$  signaling acted to modulate lymphotoxin expression by staining hematopoietic cells with soluble LT $\beta$ R-Fc (León et al., 2012; Yang et al., 2014). A small proportion of B cells, CD4<sup>+</sup> T cells, and to a lesser extent CD8<sup>+</sup> T cells from the mLN of naive mice expressed LT $\beta$ R ligands, and this increased in all populations following *Hpb* infection of WT but not IL-4R $\alpha$ <sup>-/-</sup> mice (Figures 5E, 5F, and S5C–S5G). Among these, isotype switched and germinal center B cells represented the greatest majority of lymphotoxin-expressing cells (Figure 5G). The LT $\beta$ R ligand present on B cells in *Hpb*-infected mice was confirmed as lymphotoxin, and not LIGHT, as LT $\beta$ R-Fc binding could be completely reversed by inclusion of a blocking anti-LT $\beta$  monoclonal antibody (mAb) (Figure S5H). To investigate whether IL-4 could act directly on B cells to promote lymphotoxin expression, we activated purified naive B cells in vitro by cross-linking surface IgM in the presence or absence of IL-4. Stimulation of naive B cells with anti-IgM resulted in enhanced expression, and this was further amplified by addition of IL-4, but not interferon (IFN)- $\gamma$  (Figure 5H). These results demonstrate a role for IL-4R $\alpha$  in indirectly promoting lymphoid stromal expansion and remodeling and raise the possibility that this occurs via the ability of IL-4 to promote B cell lymphotoxin expression.

#### B Cells Represent the Primary Source of Lymphotoxin Required for FRC Expansion and Remodeling

To further investigate whether B cell expressed lymphotoxin is necessary for stromal cell expansion and lymphoid remodeling following *Hpb* infection, we utilized a mixed bone marrow

#### Figure 2. *Hpb* Infection Promotes the Expansion and Re-organization of Stromal Cells in the mLN

C57BL/6J mice were infected with *Hpb*, and the entire chain of the mLN was collected at 0 (naive), 12, and 21 dpi. (A–E) CD45<sup>-</sup> stromal cell populations (frequency of total live cells) (A), fibroblastic reticular cells (FRC, Pdpn<sup>+</sup>CD31<sup>+</sup>) (B), lymphatic endothelial cells (LECs, Pdpn<sup>+</sup>CD31<sup>+</sup>) (C), blood endothelial cells (BECs, Pdpn<sup>-</sup>CD31<sup>+</sup>) (D), and double-negative (DN, Pdpn<sup>-</sup>CD31<sup>-</sup>) cells (E) in mLN. All data were determined using flow cytometry; values represent mean  $\pm$  SEM (n = 8–12 mice) and are pooled from three independent experiments. (F) Representative dot plot analysis of FRCs (pre-gated on live cells that are CD45<sup>+</sup>TER119<sup>-</sup>Pdpn<sup>+</sup>Ki67<sup>+</sup>CD31<sup>+</sup>) showing the frequency of proliferating FRCs (Ki67<sup>+</sup>Pdpn<sup>+</sup>). Each panel represents one individual mouse. (G) Whole mLN cryosections showing single and combined stainings for the stromal network represented by FRCs as defined by Pdpn (red) and PDGFR- $\alpha$  (green) positivity. Scale bar, 1,000  $\mu$ m. (H) Confocal images showing a 3D view of FRC (ER-TR7<sup>+</sup>) remodeling around B cell follicles. Images are representative of five different experiments with n  $\geq$  2 mice/group/time point. Pdpn, podoplanin; B, B cell follicle; T, T cell zone. Scale bar, 100  $\mu$ m. See also Figure S2 and Movies S2 and S3.

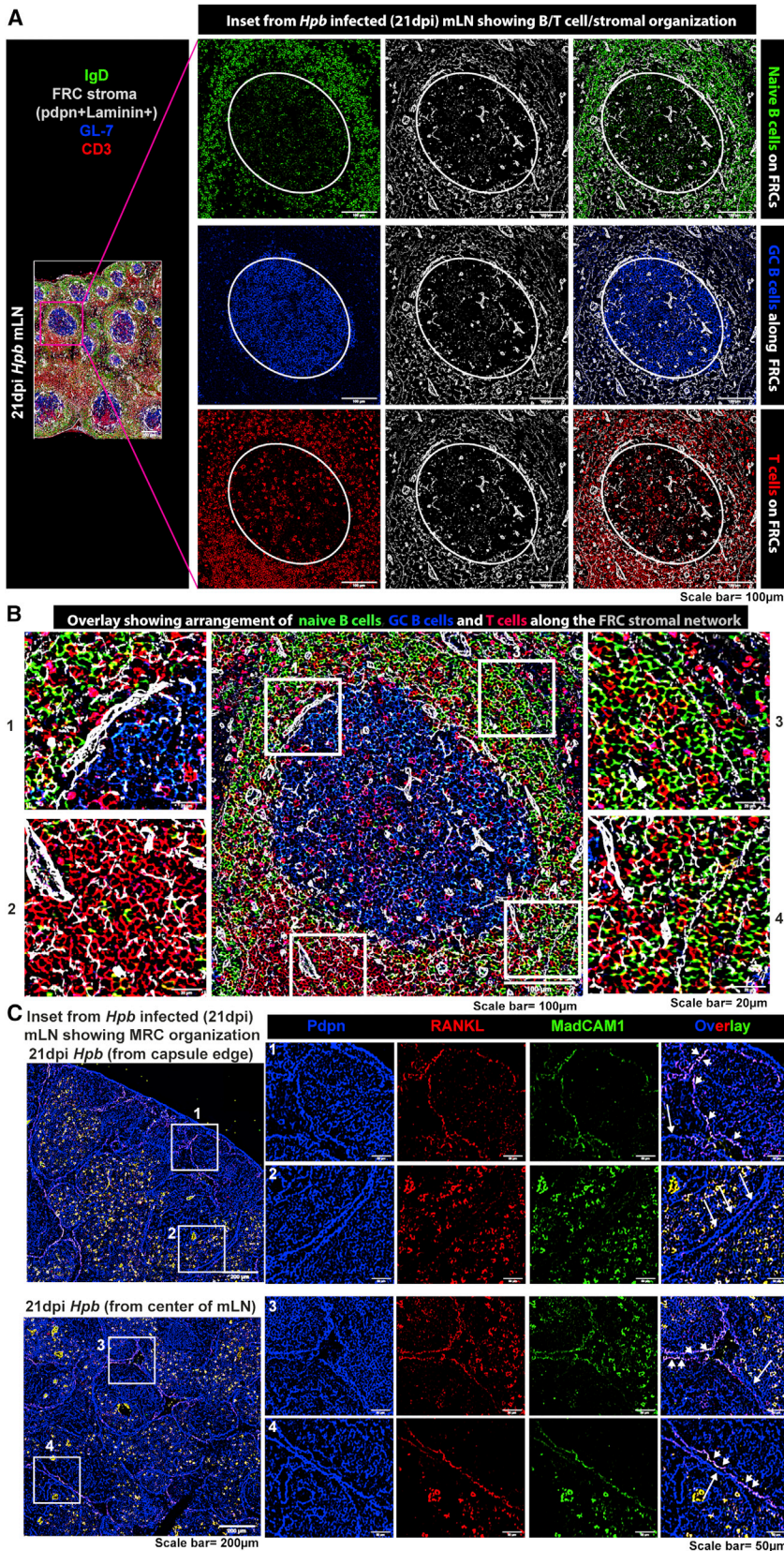


**Figure 3. FRCs Provide a Scaffold for B and T Cells within the Mantle of Follicles Present in the mLN of *Hpb*-Infected Mice**

C57BL/6J mice were infected with *Hpb*, and the entire chain of the mLN was collected at 21 dpi.

(A) mLN cryosections showing single and combined immunofluorescence staining for naive B cells (green, IgD<sup>+</sup>GL7<sup>-</sup>), T cells (red, CD3<sup>+</sup>), germinal center B cells (blue, IgD<sup>-</sup>GL7<sup>+</sup>), and FRCs (white, IgD<sup>-</sup>GL7<sup>-</sup>CD3<sup>-</sup>Pdpn<sup>+</sup>laminin<sup>+</sup>). The white circles represent the outer border of the B cell germinal center (GC). Scale bar, 100 µm.

(B) Combined overlay immunofluorescence of the image depicted in the box shown in (A) detailing the cellular arrangements of naive B cells, T cells, GC B cells, and the FRC network. Box 1 shows FRCs (white) surrounding GC B cells (blue); box 2 shows FRCs (white) within the T cell (red)-rich area; boxes 3 and 4 show the interaction of naive B cells (green) with T cells (red) together with FRCs (white). Scale bar, 100 and 20 µm as shown below the images.

(C) mLN cryosections showing single and combined immunofluorescence staining for an FRC subset, marginal reticular cells (MRCs) identified as Pdpn<sup>+</sup>MadCAM1<sup>+</sup>RANKL<sup>+</sup>. Images are shown from the capsule edge (box 1) as well as from center of the mLN (boxes 2–4) for comparison. Large arrows represent the FRCs surrounding B cell follicles (as depicted in A and B), while small arrows indicate MRCs present within the same region. Scale bar, 200 and 50 µm as shown below the images. Images are representative of three different experiments with n ≥ 3 mice/group/time point.

See also Figure S3.

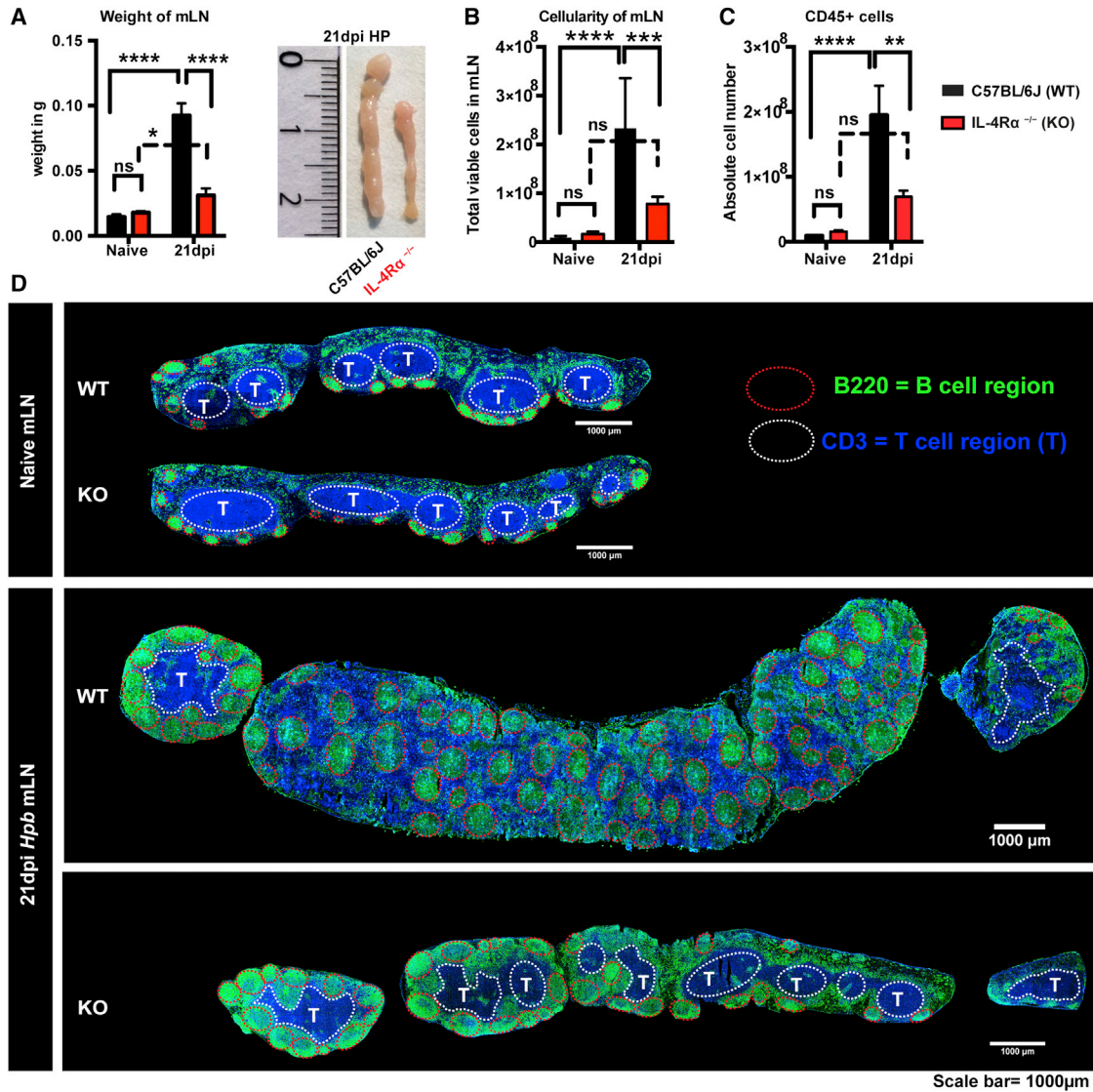


**Figure 4. mLN Swelling and De Novo Follicle Formation in Response to *Hpb* Infection Requires IL-4R $\alpha$  Signaling**

C57BL/6J (WT) and IL-4R $\alpha$ <sup>-/-</sup> (KO) mice were infected with *Hpb*, and the entire chain of the mLN was collected at day 0 (naive) and 21 dpi.

(A–C) Total weight and size (A), cellularity (B), and CD45<sup>+</sup> cell number (C) from naive or infected mice. Data are pooled from two independent experiments (n = 3–6 mice per group) and represent mean  $\pm$  SEM. nd, not detectable. \*p < 0.05, \*\*p < 0.01, \*\*\*p < 0.001, and \*\*\*\*p < 0.0001 (ANOVA, Bonferroni's multiple comparison test).

(D) mLN cryosections showing combined immunofluorescence staining for B cells (B220, green) and T cells (CD3, blue). Images are representative of three or more experiments with at least three mice/group/time point. The areas outlined in dotted white lines represent the intact central T cell zone; while red circles represent B cell follicles. Scale bar, 1,000  $\mu$ m.

See also Figure S4.

chimera approach in which lethally irradiated wild-type (WT) mice were reconstituted with bone marrow cells from B cell-deficient (JHT<sup>-/-</sup>) or T cell-deficient (TCR $\beta$  $\delta$ <sup>-/-</sup>) mice and mixed with bone marrow cells from LT $\beta$ <sup>-/-</sup> mice at a 5:1 ratio. This resulted in the generation of animals in which either B cells (JHT<sup>-/-</sup> + LT $\beta$ <sup>-/-</sup>) or T cells (TCR $\beta$  $\delta$ <sup>-/-</sup> + LT $\beta$ <sup>-/-</sup>) specifically lacked the ability to express surface lymphotoxin. Mixed bone marrow chimeras using WT donors were also generated as controls (JHT<sup>-/-</sup> + WT and TCR $\beta$  $\delta$ <sup>-/-</sup> + WT).

All groups of mice exhibited a normal lymphoid structure with T and B cell segregation and FRC-rich paracortical T cell zone under naive conditions (Figure S6A). Strikingly, mice in which B cells selectively lacked lymphotoxin failed to form new centrally located B cell follicles (Figure 6A) containing FDC positive germinal centers (Figures 6B and S6B) following *Hpb* infection. These animals also failed to expand the FRC network in response to *Hpb* infection (Figures 6A–6C), and FRCs did not re-organize to surround the B cell follicles (Figure 6D). By

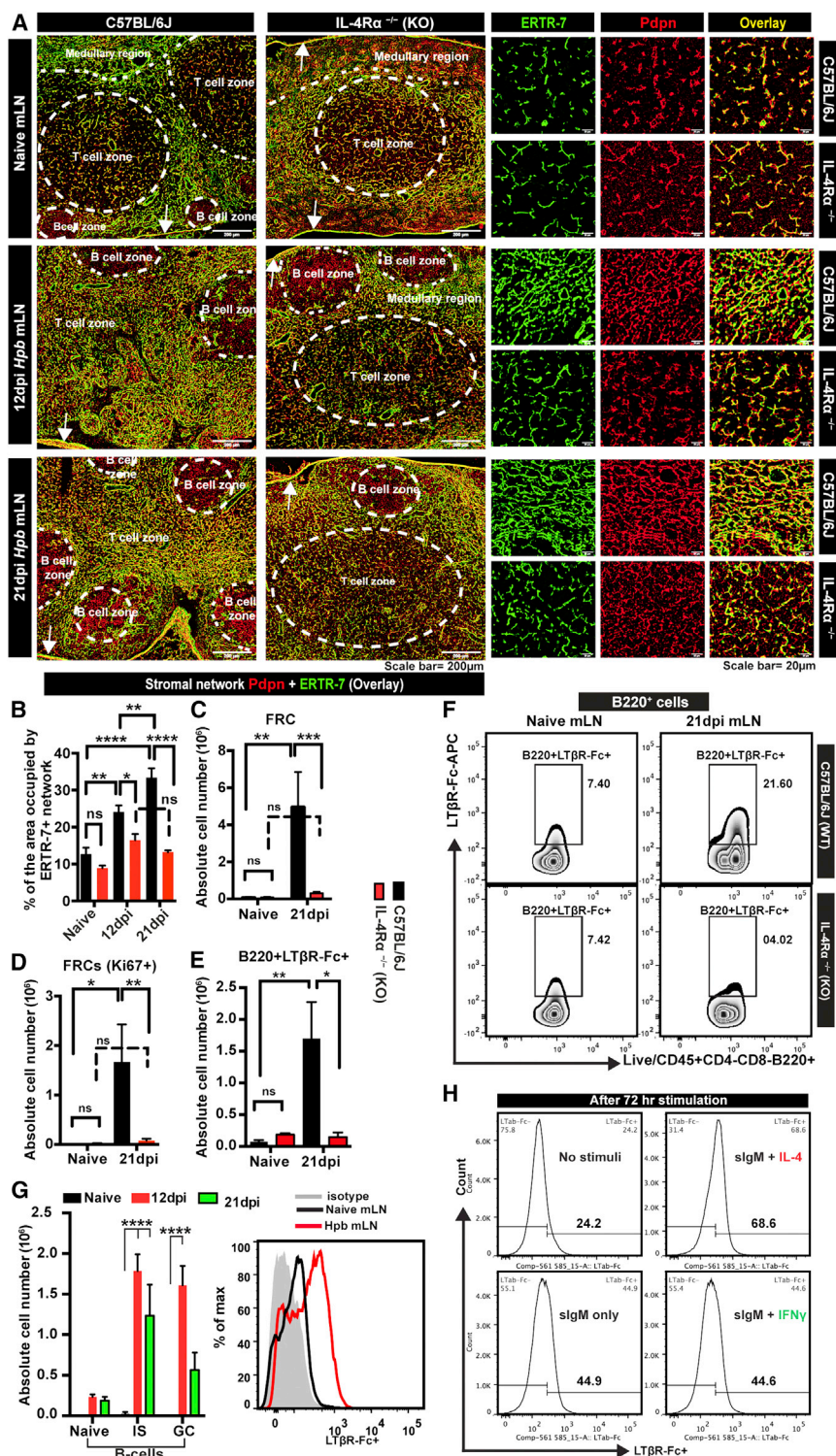


### Figure 5. FRC Expansion and Re-organization in Response to *Hpb* Infection Requires IL-4R $\alpha$ Signaling, which Promotes Lymphotoxin Expression on Lymphocytes

C57BL/6J (WT) and IL-4R $\alpha$ <sup>-/-</sup> (KO) mice were infected with *Hpb*, and the entire chain of the mLN was collected at day 0 (naive), 12, and 21 dpi.

(A) Immunofluorescence images showing stromal reticular network as defined by Pdpn (red) and ETR7 (green) expression. Insets show higher magnification of stromal reticular fibers within the T cell zone. Images are representative of four or more experiments with at least three mice/group/time point. Scale bar, 200 and 20  $\mu$ m.

(B) Quantitation of the mLN area occupied by ETR7<sup>+</sup> reticular fibers. Data represent mean  $\pm$  SEM (n = 4–6 images/mLN from two mice/time point).

(C and D) FRC number (C; live cells, CD45<sup>+</sup>Pdpn<sup>+</sup>CD31<sup>-</sup>) and FRC proliferation (D; Pdpn<sup>+</sup>CD31<sup>-</sup>Ki67<sup>+</sup>) were determined by flow cytometry with gating on Pdpn<sup>+</sup>CD31<sup>-</sup> cells. Data represent mean  $\pm$  SEM and are representative of three independent experiments with n  $\geq$  2–4 mice per group. \*p < 0.05, \*\*p < 0.01, \*\*\*p < 0.001, and \*\*\*\*p < 0.0001 (ANOVA, Bonferroni's multiple comparison test).

(E and F) Absolute cell numbers of B cells (E) and representative contour plots (F) showing flow cytometry analysis of the ability of B220<sup>+</sup> B cells to bind LTβR-Fc chimeric protein. Each panel represents one individual mouse and is representative of three independent experiments (n = 3–5 mice per group/time point).

(G) Absolute cell numbers of IgM<sup>+</sup>IgD<sup>+</sup> naive B cells, IgM<sup>-</sup> isotype switched (IS) B cells or GL7<sup>+</sup> germinal center (GC) B cells exhibiting positive staining for LTβR-Fc.

(H) LTβR-Fc binding to B cells cultured in vitro in the presence of sIgM (10  $\mu$ g/ml) and IL-4 or IFN- $\gamma$  (10 ng/ml). Data are representative of three independent experiments (n = 3–5 mice per group/time point). \*p < 0.05, \*\*p < 0.01, \*\*\*p < 0.001, and \*\*\*\*p < 0.0001 (ANOVA, Bonferroni's multiple comparison test).

See also Figure S5.

crucial role in promoting FRC expansion and de novo follicle formation in response to *Hpb* infection.

### LTβR Expression by CCL19<sup>Cre</sup> Positive Stromal Cells Is Necessary for Lymph Node Remodeling and Antibody Production following Intestinal Helminth Infection

In order to assess the contribution of de novo follicle formation to antibody production, we made use of a BAC transgenic mouse model that drives expression of the Cre recombinase under the control of the CCL19 promoter (CCL19<sup>Cre</sup>) known to be selectively active in FRCs (Chai et al., 2013). CCL19<sup>Cre</sup> mice were crossed to

contrast, mice specifically lacking lymphotoxin expression on T cells were indistinguishable from their control counterparts (Figures 6A–6D and S6). Taken together, these data indicate that B cell-derived, but not T cell-derived, lymphotoxin plays a

duction, we made use of a BAC transgenic mouse model that drives expression of the Cre recombinase under the control of the CCL19 promoter (CCL19<sup>Cre</sup>) known to be selectively active in FRCs (Chai et al., 2013). CCL19<sup>Cre</sup> mice were crossed to

LT $\beta$ R<sup>fl/fl</sup> mice to generate animals in which the LT $\beta$ R was selectively lost on FRCs. CCL19<sup>-cre</sup>  $\times$  LT $\beta$ R<sup>fl/fl</sup> mice exhibited a severely impaired ability to generate new B cell follicles following *Hpb* infection (Figures 7A and 7C), and those follicles that did form contained less FDCs compared to wild-type mice (Figures S7A–S7D). CCL19<sup>-cre</sup>  $\times$  LT $\beta$ R<sup>fl/fl</sup> mice also exhibited a reduced ability to expand and reorganize FRCs around B cell follicles (Figures 7B and S7E–S7H). This coincided with reduced lymph node swelling (Figure 7D) and attenuated production of both total and helminth-specific IgG1 (Figures 7E and 7F) and IgE (Figures 7G and 7H) antibodies. These data validate our earlier findings that lymphoid remodeling and de novo follicle formation requires stromal cell activation via the LT $\beta$ R pathway. They further indicate that de novo follicle formation is necessary for the efficient production of antibodies in response to helminth infection.

Interestingly, examination of the intestines of CCL19<sup>-cre</sup>  $\times$  LT $\beta$ R<sup>fl/fl</sup> mice revealed that these mice also developed fewer type 2 granulomas (Figure 7I), although this did not reach significance. They also harbored greater numbers of adult worms at late time points following infection when the host normally begins to expel these organisms (Figure 7J). Both granuloma development and worm expulsion are known to be dependent on effector Th2 cells following primary infection with *Hpb* (Anthony et al., 2006; Morimoto et al., 2004), indicating that CCL19<sup>-cre</sup>  $\times$  LT $\beta$ R<sup>fl/fl</sup> mice also failed to properly activate effector CD4<sup>+</sup> Th2 cells.

## DISCUSSION

The initiation of adaptive immune responses relies on inflammatory cues and involves the accumulation of increased numbers of T and B cells within the draining lymph node. These changes go hand in hand with an expansion of the stromal cell network that both guides and accommodates the lymphocyte influx. Here, we report that IL-4R $\alpha$ -dependent type 2 inflammation, resulting from intestinal helminth infection, drives both the swelling and cellular re-organization of the draining mLN. We provide evidence that infection induced mLN remodeling requires IL-4R $\alpha$  signaling, which functions to promote lymphotoxin expression by hematopoietic cells. Bone marrow chimeras specifically lacking lymphotoxin expression on B cells revealed a critical role for interaction of these cells with LT $\beta$ R-expressing CCL19<sup>+</sup> stromal cells. B cell-stromal cell interactions were necessary for stromal cell expansion and de novo follicle formation, which together functioned to promote antibody production in response to helminth infection.

Immunity to *Hpb* requires IL-4R $\alpha$  (Wojciechowski et al., 2009), and CXCR5-expressing DCs and T cells localize adjacent to B cell areas to promote Th2 differentiation (León et al., 2012). Our study supports these findings and additionally provides new data revealing a role for IL-4R $\alpha$  signaling to B cells to promote lymphotoxin expression that allows B cell-stromal cell crosstalk. Such crosstalk was necessary for lymph node enlargement, stromal cell proliferation, and the formation of the new centrally located B cell follicles that supported antibody production. FRCs are known to form conduits that deliver small antigens to the T cell zone and to B cell follicles (Rozen daal et al., 2009); thus, it is likely that the dense FRC networks we observe in

the follicle mantle also serve to deliver soluble parasitic antigens to the germinal center. The presence of a FRC conduit network around newly formed B cell follicles may be particularly relevant for *Hpb* infection as the adult worm is localized within (and limited to) the small intestinal lumen, and the most highly immunogenic proteins are found within its secreted products (Grainger et al., 2010; Hewitson et al., 2013; Massacand et al., 2009).

De novo formation of B cell follicles has only previously been reported during neonatal lymphoid organogenesis where B cells enter T cell-rich lymph nodes, a few weeks after birth, to form new B cell follicles (Bajénoff and Germain, 2009). Follicle formation during lymphoid organogenesis also involves lymphotoxin-expressing B cells that provide signals to LT $\beta$ R-expressing stromal cells (Gonzalez et al., 1998; Kumar et al., 2010), with the newly arrived B cells displacing the existing T cells and FRCs thus creating a “cortical ridge” that surrounds the newly formed follicle (Katakai et al., 2004). Whether this phenomenon in adult mice is limited to settings of type 2 inflammation, or whether it also occurs in response to other stimuli (i.e., type 1 inflammation) remains to be determined. B cell follicles have been reported to trespass into the T cell zone in response to adjuvant elicited inflammation (Mionnet et al., 2013), and León et al. (2012) have previously reported that DCs and T cells re-localize near B cell areas following *Hpb* infection, although this was not observed following influenza infection (León et al., 2012). Although IFN- $\gamma$  expression has been previously reported to promote lymphotoxin expression on CD4<sup>+</sup> T cells (Luther et al., 2002; Schneider et al., 2004), we did not observe a role for IFN- $\gamma$  in promoting lymphotoxin expression on B cells activated in vitro. Nevertheless, it would of great interest to investigate the impact of type 1 inflammation on mLN re-organization and de novo follicle formation following intestinal infection with bacterial or viral pathogens.

Although it is not clear exactly how new B cell follicles are formed in response to *Hpb*, it is likely that B cell-expressed lymphotoxin also activates MRCs as we observed a dramatic expansion and migration of these cells in *Hpb*-infected mLN. MRCs and FRCs are thought to arise from a common precursor, and their development during lymphoid organogenesis relies on LT $\beta$ R signaling (Rozen daal and Mebius, 2011), with MRCs also able to transform into FDCs (Jarjour et al., 2014). FDCs can produce CXCL13 in response to LT $\beta$ R signaling (Katakai et al., 2008; Rozen daal and Mebius, 2011), and this cytokine is crucial for follicle establishment and B cell retention within germinal centers (Wang et al., 2011). We observed reduced FDC-containing follicles and CXCL13 production in the absence of IL-4R $\alpha$  signaling, raising the possibility that IL-4R $\alpha$ -mediated upregulation of lymphotoxin expression by B cells following *Hpb* infection promotes de novo follicle formation by driving MRC expansion, migration, and conversion to FDCs. Our hypothesis that IL-4 signaling promotes stromal cell remodeling via the action of IL-4 on B cells is supported by data showing that IL-4 promotes lymphotoxin expression on B cells in vitro, and our finding that *Hpb*-induced B cell lymphotoxin expression is abrogated in IL-4R $\alpha$ -deficient mice. However, it would be of great interest to investigate the impact of *Hpb* infection on mice that lack IL-4R $\alpha$  specifically on B cells in order to validate the relevance of this pathway for stromal cell activation and remodeling in vivo.

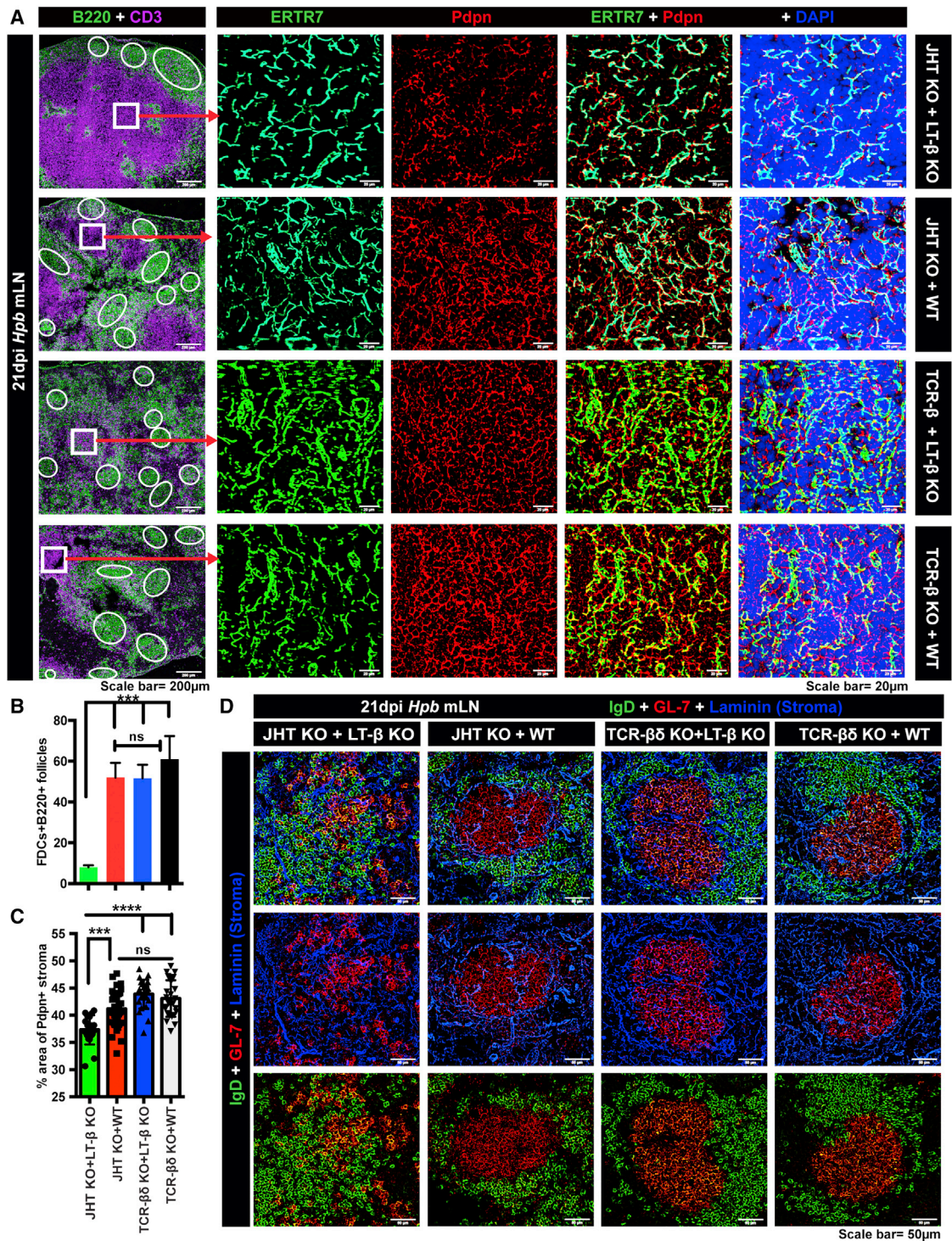


**Figure 6. B Cell-Derived Lymphotoxin Is Required for De Novo Follicle Formation and T Cell Zone Stromal Cell Expansion in Response to *Hpb* Infection**

Mixed bone marrow chimeras were generated using lethally irradiated wild-type (WT) recipients reconstituted with bone marrow cells from B cell-deficient (JHT<sup>-/-</sup>) or T cell-deficient (TCRβδ<sup>-/-</sup>) mice mixed with bone marrow cells from LTβ<sup>-/-</sup> mice at a 5:1 ratio. Resulting animals lacked surface lymphotoxin expression on B cells (JHT<sup>-/-</sup> + LTβ<sup>-/-</sup>) or T cells (TCRβδ<sup>-/-</sup> + LTβ<sup>-/-</sup>) and were compared to control mice receiving B or T cell-deficient bone marrow mixed with WT bone marrow cells (JHT<sup>-/-</sup> + WT and TCRβδ<sup>-/-</sup> + WT). All mice were infected with *Hpb*, and the entire chain of the mLN was collected at day 0 (naive) and 21 dpi.

(legend continued on next page)

Lymphotoxin-expressing B cells also interact directly with FRCs to promote FRC expansion and remodeling, such that these cells form a ring around the follicle mantle where they interact extensively with both T and B cells. Lymphotoxin-dependent B cell-stromal cell crosstalk was crucial for effective immunity against *Hpb*, as infection of CCL19<sup>-cre</sup> × LTβR<sup>fl/fl</sup> mice resulted in a failure to expel the parasite at late time points post infection, and also lead to a reduction in the formation of new B cell follicles and the production of IgG1 and IgE antibodies. CCL19<sup>-cre</sup> × LTβR<sup>fl/fl</sup> mice have previously been shown to form lymph nodes and to normally segregate the T and B cell compartments under naive conditions (Chai et al., 2013), and this finding was confirmed in our present study. Thus, a requirement for LTβR signaling on CCL19<sup>+</sup> stromal cells distinguishes de novo follicle formation in response to helminth infection as being distinct from that occurring during neonatal lymphoid organogenesis.

Attenuation of both de novo follicle formation and antibody production in CCL19<sup>-cre</sup> × LTβR<sup>fl/fl</sup> mice indicates that de novo follicle formation functions to support antibody production. While antibodies have little impact on the expulsion of adult worms following primary *Hpb* infection (McCoy et al., 2008), they are crucial for resistance of immune mice against repeated infections with the parasite. This is especially important for intestinal helminths, as the large majority of parasitic helminth species do not replicate within their host and parasite burdens within a host increase as a result of constant re-infection. De novo follicle formation may also serve to increase the area of T-B cell interaction thus promoting the establishment of an effector Th2 response (León et al., 2012). This hypothesis is in keeping with our observation that CCL19<sup>-cre</sup> × LTβR<sup>fl/fl</sup> mice exhibited increased worm burdens following primary infection when worm expulsion is primarily driven by type 2 cytokines. Although the studies reported here were limited to the impact of B cell-stromal cell crosstalk on FRC expansion and follicle formation, it would also be of great interest to investigate the impact of LTβR-mediated FRCs activation on other immune parameters, or whether FRCs and B cells additionally talk to other stromal cell types.

While lymphoid remodeling and de novo follicle formation appear to enhance immunity against *Hpb*, it is unclear whether this would have a beneficial or detrimental impact on heterologous immune responses occurring against unrelated intestinal pathogens and antigens. Further exploration in this area would be of high interest given the frequency and perceived importance of co-infections on host immunity. Indeed, important pathogens

like *Plasmodium* species and HIV often overlap in geographic distribution with intestinal helminths (Mulu et al., 2015; Salgame et al., 2013), and loss of FRCs has previously been associated with compromised immunity against HIV infection (Zeng et al., 2011).

In summary, our data have revealed a role for IL-4Rα signaling in promoting lymphotoxin expression by B cells that allows B cell-stromal cell crosstalk and promotes lymph node swelling and de novo follicle formation. We also show that de novo follicle formation is necessary for the development of effective adaptive immunity following intestinal helminth infection. The finding that inflammation can drive the formation of new B cell follicles in adult lymphoid organs may have wide ranging implications for our understanding of lymphoid plasticity and the generation of effective antibody responses against other pathogens, or in response to vaccination.

## EXPERIMENTAL PROCEDURES

### Ethics Statement

All animal experiments were approved by the Service de la consommation et des affaires vétérinaires (1066 Épalinges, Canton of Vaud, Switzerland) with the authorization numbers VD 2238.1, VD 3001, and VD1612.3.

### Mice Strains, Parasites, and Treatments

C57BL/6J (WT) mice were obtained from Charles River Laboratories. JHT<sup>-/-</sup>, IL-4Rα<sup>-/-</sup> mice were bred and maintained on the C57BL/6J background under specific pathogen-free (SPF) conditions at École Polytechnique Fédérale de Lausanne (EPFL), Switzerland. LT-β<sup>-/-</sup> and TCRβδ<sup>-/-</sup> mice (C57BL/6J background) were maintained at the Épalinges animal facility, University of Lausanne, Switzerland. Stromal cell-specific LTβR<sup>-/-</sup> mice (CCL19<sup>-cre</sup> × LTβR<sup>fl/fl</sup>) were described previously (Chai et al., 2013). All experimental mice were aged between 8 and 12 weeks and both age and sex matched for individual experiments. Mice subjected to intestinal helminth infection were given 200 L3 stage parasites by oral gavage and sacrificed at 12 or 21 days post-infection (dpi). Parasite numbers were determined by counting of adult worms within the intestine and its contents using a stereomicroscope.

### Enzymatic Digestion of Mesenteric Lymph Nodes

For flow cytometric analysis, mLN were processed as previously described with slight modifications (Cremasco et al., 2014; Fletcher et al., 2011). Briefly, mLN from individual mice were dissected and placed in cold RPMI-1640 on ice. After all lymph nodes were dissected, the RPMI-1640 was removed and replaced with 3–5 ml of freshly made digestion mixture comprised of RPMI-1640 containing 0.8 mg/ml Dispase, 0.2 mg/ml Collagenase P (both from Roche), and 0.1 mg/ml DNase I (Invitrogen). Tubes were incubated at 37°C and gently inverted at 10-min intervals to ensure the contents were well mixed. After 15 min, lymph nodes were gently dispersed into a single-cell suspension using a 1-ml pipette. The large fragments were allowed to settle for 60 s, after which the enzyme mix was complemented with 5 ml of ice-cold FACS buffer

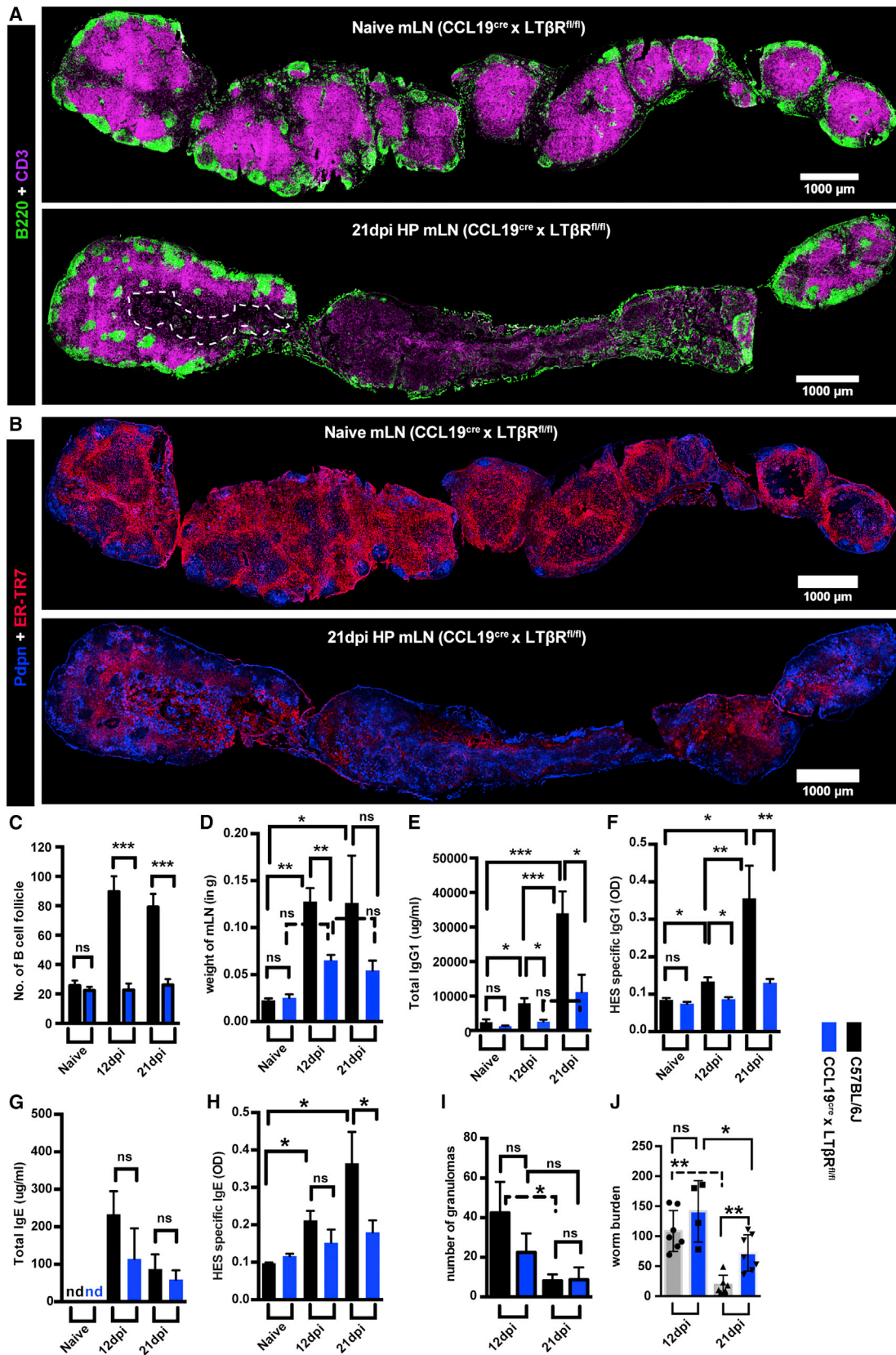
(A) mLN cryosections from infected mice showing combined immunofluorescence images staining for B cells (B220, green) and T cells (CD3, magenta). Higher magnification images show the boxed area within the T cell zone and were stained for stromal cells as defined by expression of Pdpn (red) and the matrix marker ERTR-7 (green). Nuclei are counterstained using DAPI (blue).

(B) The total number of B cell follicles (B220<sup>+</sup>) that were also positive for FDCs (FDC-M1<sup>+</sup>) were determined on a graphic tablet at higher magnification, and data are presented as mean ± SEM (n = 4 mLN/time point).

(C) Immunofluorescence images from the T cell zone of infected mLN were acquired and segmented using ImageJ software, and the number of pixels specific for Pdpn<sup>+</sup> in the T cell zone was determined and expressed as the percentage of total pixels in each area occupied by Pdpn. Data represent mean ± SEM. Each symbol represents an individual T cell zone. The total numbers of T cell zones (n = 19–37) used for quantification were pooled from three different lymph nodes for each group.

(D) Combined overlay immunofluorescence images from infected mLN showing naive B cells (green, IgD<sup>+</sup>) and germinal center B cells (red, GL7<sup>+</sup>) together with stromal cell associated matrix (blue, Laminin<sup>+</sup>). Scale bar, 50 μm.

See also Figure S6.



(legend on next page)

(2% fetal calf serum [FCS], 5 mM EDTA in PBS) before centrifugation (1,200 rpm, 5 min, 4°C). 5 ml of fresh enzyme mix was added to the digestion tube, and the digestion mix was vigorously mixed using a 1 ml pipette every 5 min until it was clear that all remaining lymph node fragments were completely digested. The cells were filtered through a 40- $\mu$ m cell strainer, counted, and used for FACS staining.

#### Flow Cytometry and Antibodies

After the enzymatic digestion of mLN, cells were resuspended in FACS buffer (PBS containing 2% FBS and 5 mM EDTA) and were incubated for 30 min with antibodies to the various markers as detailed in [Table S1](#). The samples were acquired on a BD-LSRII machine and analyzed using FlowJo (v.10.0.6).

#### Histology and Immunofluorescence Microscopy

The entire length of the mesenteric lymph node chain was carefully dissected, weighed, imaged, and embedded in Tissue-Tek optimum cutting temperature compound (OCT) (Thermo Scientific) and then frozen in an ethanol dry ice bath. Serial cryostat sections (8  $\mu$ m in thickness) were collected over a span of 400  $\mu$ m depth on Superfrost Plus glass slides (Fisher Scientific), air-dried, and fixed for 10–15 min in ice-cold acetone. After rehydration in PBS, sections were blocked with 1% (w/v) BSA and 1%–4% (v/v) normal mouse and donkey serum, followed by treatment with a streptavidin-biotin blocking kit (Vector Laboratories). Immunofluorescence staining was performed using antibodies (listed in [Table S2](#)) diluted in PBS containing 1% (w/v) BSA and 1% (v/v) normal mouse serum. Sections were incubated with primary antibodies overnight at 4°C. The following day, sections were washed three times in PBS, and primary antibodies were detected by incubating sections with fluorescently labeled secondary antibodies, and nuclei were counterstained with DAPI prior to mounting of the sections using ProLong anti-fade reagents (Life Technologies). Stained sections were then imaged after 24 hr.

#### Image Acquisition and Processing

Images were acquired on an Olympus VS120-SL full slide scanner using a 20 $\times$ /0.75 air objective and an Olympus XM10 B/W camera or LSM710 (20 $\times$ /1.2 or 40 $\times$ /1.4) using regular photomultiplier tubes (PMTs), 1-a.u. pinhole, Z spacing 1–10  $\mu$ m) laser scanning confocal microscope. Each image was acquired using the indicated fluorescent channels and the same exposure time/PMT gain employed across different samples. The resulting image file ( $\approx$  1 GB) (.VSI) was downsampled when extracted using the VSI reader action bar developed by the EPFL BiImaging & Optics Platform (BIOP). For generation of the final images comparing different samples (i.e., naive versus infected mLN), the images were further downsampled (4 $\times$ ), each fluorescent channel was set to the same brightness and contrast, the lymph node chain was outlined, and the channels were montaged using ImageJ/Fiji such that the final image represented the individual and overlay of all channels. Alternatively, images were directly processed using Olympus slide scanner software (OlyVIA v.2.6) after adjusting the brightness and contrast settings so that they remained the same across all samples compared. For quantitative measurements, immunofluorescence images from naive and infected mice mLN were acquired using LSM710 confocal microscope and segmented using the ImageJ/Fiji pipeline. A threshold-based approach was used to measure the areas specific for podoplanin or ERTR-7 and expressed as the percentage of total area occupied by

the given marker. For quantifying the number of B cell follicles, mLN sections were stained with anti-B220, anti-CD35, and/or anti-GL7 antibody and were imaged using Olympus slide scanner. After image acquisition, B cell follicles were counted at high magnification using a graphic tablet based on B220<sup>+</sup> staining. For each group, data were pooled from two independent experiments ( $n = 2$  to 3 mLN/time point/experiment) and represented as mean  $\pm$  SEM. The ImageJ/Fiji macros are available on demand. The final figure panels (graphs and images) were arranged and converted to .TIF file (LZW compression) using Adobe Photoshop CS5.

#### Vibratome Sections

Isolated mLN were fixed overnight at 4°C in freshly prepared 1% paraformaldehyde in PBS, washed, and embedded in 2% (w/v) low-melting agarose (Sigma-Aldrich) in PBS. 500- $\mu$ m sections were cut with a vibratome (Microm HM 650V) and were used for staining. These thick sections were blocked with blocking buffer (as described previously) overnight and stained for at least 96 hr with the primary antibodies listed in [Table S2](#), followed by extensive washing in PBS before incubation with fluorescently labeled secondary antibodies. After staining, samples were cleared using fructose as described previously ([Ke et al., 2013](#)). After clearing, vibratome sections were imaged using light sheet microscope (Zeiss) with 20 $\times$  objective in a 80.2% fructose solution. The 3D reconstruction and movies were made using IMARIS (Bitplane).

#### Bone Marrow Chimeras

Bone marrow (BM) from donor mice was obtained from the femur and tibia by crushing bones with a mortar. BM cells were injected intravenously into C57BL/6J (WT) recipient mice previously irradiated two times with 450 rad with a 4-hr interval. All mice were maintained in specific pathogen-free conditions. For the generation of mice in which B cells lack lymphotoxin expression (B-*Lt $\beta$ <sup>-/-</sup>*) and B-WT chimeras, C57BL/6J recipients were reconstituted with 80% JHT bone marrow plus 20% *Lt $\beta$ <sup>-/-</sup>* bone marrow or with 80% JHT bone marrow plus 20% WT bone marrow, respectively. For the generation of mice in which T cells lack lymphotoxin expression (T-*Lt $\beta$ <sup>-/-</sup>*) and T-WT chimeras, C57BL/6J recipients were reconstituted with 80% TCR- $\beta\delta$  bone marrow plus 20% *Lt $\beta$ <sup>-/-</sup>* bone marrow or with 80% TCR- $\beta\delta$  bone marrow plus 20% WT bone marrow. Mice received the antibiotic “Baytril 10%” (1/1,000) in the drinking water for 4–8 weeks following bone marrow reconstitution and were subjected to *Hpb* infection at 8–12 weeks following reconstitution.

#### ELISAs

Serum titers of total or *Hpb* L5 excretory secretory products (HES) reactive IgG1 and IgE were determined as previously described ([McCoy et al., 2008](#)). Briefly, Nunc MaxiSorp 96-well plates were coated with either 1  $\mu$ g/ml anti-IgE (BioLegend 406902), 5  $\mu$ g/ml anti-IgG1 (Southern Biotech 1070-01) or 1–10  $\mu$ g/ml HES, and incubated overnight at 4°C. Serum samples were added the next day and incubated overnight at 4°C, before the addition of 1  $\mu$ g/ml alkaline-phosphatase-conjugated anti-IgE (Southern Biotech 1130-04) or anti-IgG1 (Southern Biotech 1070-06). 4-Nitrophenyl phosphate sodium salt hexahydrate (Sigma) was used as a substrate and the colorimetric reaction was read at 405 nm on a Benchmark Plus spectrophotometer (Bio-Rad).

### Figure 7. *LT $\beta$ R* Expression by *CCL19<sup>-cre</sup>* Positive Stromal Cells Is Required for mLN Swelling De Novo Follicle Formation and Antibody Production following *Hpb* Infection

(A and B) *CCL19<sup>-cre</sup>  $\times$  LT $\beta$ R<sup>fl/fl</sup>* mice were infected with *Hpb*, and the entire chain of the mLN collected at day 0 (naive), 12, and 21 dpi. (A) mLN cryosections from naive and 21 dpi showing combined immunofluorescence staining for B cells (B220, green) and T cells (CD3, magenta) are shown. Images are representative mLN sections collected from two independent experiments with at least  $n = 2$ –3 mice/group/time point. Scale bar, 1,000  $\mu$ m. (B) mLN cryosections from naive and 21 dpi showing combined immunofluorescence staining for Pdpn (blue) and ER-TR7 (red) are shown. Images are representative mLN sections collected from two independent experiments with at least  $n = 2$ –3 mice/group/time point. Scale bar, 1,000  $\mu$ m.

(C–J) *CCL19<sup>-cre</sup>  $\times$  LT $\beta$ R<sup>fl/fl</sup>* and C57BL/6 mice were infected with *Hpb* and mice sacrificed at day 0 (naive), 12, or 21 dpi. (C) The number of B cell follicles in mLN cryosections were counted on a graphic tablet at higher magnification as described in [Figure 1](#). (D) mLN weight. (E–H) Serum was collected at day 0, 12, and 21 dpi, and antibody levels for (E) total IgG1, (F) HES-specific IgG1, (G) total IgE, and (H) HES-specific IgE were determined by ELISA. Intestinal granulomas (I) and adult intestinal worm numbers (J) were determined at 12 and 21 dpi as described in [Experimental Procedures](#). (C–J) All data are pooled from two independent experiments and expressed as mean  $\pm$  SEM  $n = 3$ –6 mice per group. \* $p < 0.05$ , \*\* $p < 0.01$ , \*\*\* $p < 0.001$ , and \*\*\*\* $p < 0.0001$  (Mann-Whitney test).

See also [Figure S7](#).

### In Vitro B Cell Stimulation

Freshly purified mesenteric lymph node B cells (B220 negative selection kit; Miltenyi) were cultured in complete RPMI-1640 medium overnight before stimulation. After overnight resting phase cells were stimulated in presence of sIgM (10  $\mu$ g/ml) (AffiniPure F(ab)<sub>2</sub> fragment goat anti-mouse IgM, Jackson ImmunoResearch) with or without rIL-4/rIFN- $\gamma$  (10 ng/ml), PeproTech. After 72 hr of culture cells were washed twice with PBS and stained for surface LT $\beta$ R-Fc as described previously (Yang et al., 2014).

### RNA Isolation and qRT-PCR Analysis

mLN were mashed through a 40- $\mu$ m filter using a 5-ml syringe plunger, with the filtered cells representing the soluble cellular part and the remaining white matter left on strainer representing stromal fraction. RNA was extracted with a Direct-zol RNA MiniPrep kit (Zymo Research) and reverse transcribed using RevertAid cDNA synthesis reagents (Thermo Scientific) for qPCR analysis. qPCR was performed using SYBR Green I Master Mix (Eurogentec) on an Applied Biosystems 7900HT System.

### Statistical Analysis

Statistical analyses were performed using a non-parametric Mann-Whitney test, one-way or two-way ANOVA as indicated and with post-tests as appropriate. p values are indicated as \*p < 0.05, \*\*p < 0.01, \*\*\*p < 0.001, \*\*\*\*p < 0.0001, or ns (statistically not significant). Graph generation and statistical analyses were performed using Prism version 6 software (GraphPad).

### SUPPLEMENTAL INFORMATION

Supplemental Information includes seven figures, two tables, and three movies and can be found with this article online at <http://dx.doi.org/10.1016/j.celrep.2016.04.023>.

### AUTHOR CONTRIBUTIONS

L.K.D. and N.L.H. conceived of and designed the study. L.K.D. performed all the experiments. L.L. performed antibody ELISAs. I.M. and C.-Y.Y. helped with the generation of bone marrow chimeras. E.S. and B.L. provided CCL19<sup>cre</sup>  $\times$  LT $\beta$ R<sup>fl/fl</sup> mice, and S.A.L. provided stromal analysis tools and reagents. B.L. and S.A.L. provided critical suggestions and feedback throughout the study. L.K.D. and N.L.H. analyzed the data and wrote the manuscript.

### ACKNOWLEDGMENTS

We thank the École Polytechnique Fédérale de Lausanne (EPFL) animal facility, Miguel Garcia and the EPFL Flow Cytometry Core Facility, Jessica Sordet-Dessimoz and EPFL Histology Core Facility for providing useful suggestions during the experiments. A special thanks to Olivier Burri and Arne Seitz from the Bio-Imaging and Optics Platform for ImageJ/Fiji tools and advice for image analysis. We also thank Biogen Idec for providing LT $\beta$ R-Fc (to S.A.L.) and anti-LT $\beta$  mAb (to N.L.H.) for lymphotoxin studies. Last, we would like to thank Leonardo Scarpellino from the University of Lausanne for his valuable help during irradiation process. This work was supported by the Leenaards prize for translational research in medicine awarded to N.L.H. and S.A.L. in 2012 by the Leenaards Foundation, Lausanne, Switzerland.

Received: September 18, 2015

Revised: February 2, 2016

Accepted: April 1, 2016

Published: May 5, 2016

### REFERENCES

Acton, S.E., Farrugia, A.J., Astarita, J.L., Mourão-Sá, D., Jenkins, R.P., Nye, E., Hooper, S., van Blijswijk, J., Rogers, N.C., Snelgrove, K.J., et al. (2014). Dendritic cells control fibroblastic reticular network tension and lymph node expansion. *Nature* 514, 498–502.

Anthony, R.M., Urban, J.F., Jr., Alem, F., Hamed, H.A., Rozo, C.T., Boucher, J.-L., Van Rooijen, N., and Gause, W.C. (2006). Memory T(H)2 cells induce alternatively activated macrophages to mediate protection against nematode parasites. *Nat. Med.* 12, 955–960.

Astarita, J.L., Cremasco, V., Fu, J., Darnell, M.C., Peck, J.R., Nieves-Bonilla, J.M., Song, K., Kondo, Y., Woodruff, M.C., Gogineni, A., et al. (2015). The CLEC-2-podoplanin axis controls the contractility of fibroblastic reticular cells and lymph node microarchitecture. *Nat. Immunol.* 16, 75–84.

Bajénoff, M., and Germain, R.N. (2009). B-cell follicle development remodels the conduit system and allows soluble antigen delivery to follicular dendritic cells. *Blood* 114, 4989–4997.

Bethony, J., Brooker, S., Albonico, M., Geiger, S.M., Loukas, A., Diemert, D., and Hotez, P.J. (2006). Soil-transmitted helminth infections: ascariasis, trichuriasis, and hookworm. *Lancet* 367, 1521–1532.

Chai, Q., Onder, L., Scandella, E., Gil-Cruz, C., Perez-Shibayama, C., Cupovic, J., Danuser, R., Sparwasser, T., Luther, S.A., Thiel, V., et al. (2013). Maturation of lymph node fibroblastic reticular cells from myofibroblastic precursors is critical for antiviral immunity. *Immunity* 38, 1013–1024.

Cremasco, V., Woodruff, M.C., Onder, L., Cupovic, J., Nieves-Bonilla, J.M., Schildberg, F.A., Chang, J., Cremasco, F., Harvey, C.J., Wucherpfennig, K., et al. (2014). B cell homeostasis and follicle confines are governed by fibroblastic reticular cells. *Nat. Immunol.* 15, 973–981.

Finkelman, F.D., Shea-Donohue, T., Morris, S.C., Gildea, L., Strait, R., Madden, K.B., Schopf, L., and Urban, J.F., Jr. (2004). Interleukin-4- and interleukin-13-mediated host protection against intestinal nematode parasites. *Immunity* 20, 139–155.

Fletcher, A.L., Lukacs-Kornek, V., Reynoso, E.D., Pinner, S.E., Bellemare-Pelletier, A., Curry, M.S., Collier, A.-R., Boyd, R.L., and Turley, S.J. (2010). Lymph node fibroblastic reticular cells directly present peripheral tissue antigen under steady-state and inflammatory conditions. *J. Exp. Med.* 207, 689–697.

Fletcher, A.L., Malhotra, D., Acton, S.E., Lukacs-Kornek, V., Bellemare-Pelletier, A., Curry, M., Armant, M., and Turley, S.J. (2011). Reproducible isolation of lymph node stromal cells reveals site-dependent differences in fibroblastic reticular cells. *Front. Immunol.* 2, 35.

Gonzalez, M., Mackay, F., Browning, J.L., Kosco-Vilbois, M.H., and Noelle, R.J. (1998). The sequential role of lymphotoxin and B cells in the development of splenic follicles. *J. Exp. Med.* 187, 997–1007.

Grainger, J.R., Smith, K.A., Hewitson, J.P., McSorley, H.J., Harcus, Y., Filbey, K.J., Finney, C.A.M., Greenwood, E.J.D., Knox, D.P., Wilson, M.S., et al. (2010). Helminth secretions induce de novo T cell Foxp3 expression and regulatory function through the TGF- $\beta$  pathway. *J. Exp. Med.* 207, 2331–2341.

Harris, N.L. (2011). Advances in helminth immunology: optimism for future vaccine design? *Trends Parasitol.* 27, 288–293.

Heesters, B.A., Myers, R.C., and Carroll, M.C. (2014). Follicular dendritic cells: dynamic antigen libraries. *Nat. Rev. Immunol.* 14, 495–504.

Hewitson, J.P., Ivens, A.C., Harcus, Y., Filbey, K.J., McSorley, H.J., Murray, J., Bridgett, S., Ashford, D., Dowle, A.A., and Maizels, R.M. (2013). Secretion of protective antigens by tissue-stage nematode larvae revealed by proteomic analysis and vaccination-induced sterile immunity. *PLoS Pathog.* 9, e1003492.

Jarjour, M., Jorquera, A., Mondor, I., Wienert, S., Narang, P., Coles, M.C., Klauschen, F., and Bajénoff, M. (2014). Fate mapping reveals origin and dynamics of lymph node follicular dendritic cells. *J. Exp. Med.* 211, 1109–1122.

Katakai, T., Hara, T., Lee, J.-H., Gonda, H., Sugai, M., and Shimizu, A. (2004). A novel reticular stromal structure in lymph node cortex: an immuno-platform for interactions among dendritic cells, T cells and B cells. *Int. Immunol.* 16, 1133–1142.

Katakai, T., Suto, H., Sugai, M., Gonda, H., Togawa, A., Suematsu, S., Ebisuno, Y., Katagiri, K., Kinashi, T., and Shimizu, A. (2008). Organizer-like reticular stromal cell layer common to adult secondary lymphoid organs. *J. Immunol.* 181, 6189–6200.

Ke, M.-T., Fujimoto, S., and Imai, T. (2013). SeeDB: a simple and morphology-preserving optical clearing agent for neuronal circuit reconstruction. *Nat. Neurosci.* 16, 1154–1161.

- King, I.L., and Mohrs, M. (2009). IL-4-producing CD4+ T cells in reactive lymph nodes during helminth infection are T follicular helper cells. *J. Exp. Med.* **206**, 1001–1007.
- Kumar, V., Scandella, E., Danuser, R., Onder, L., Nitschké, M., Fukui, Y., Halin, C., Ludewig, B., and Stein, J.V. (2010). Global lymphoid tissue remodeling during a viral infection is orchestrated by a B cell–lymphotoxin-dependent pathway. *Blood* **115**, 4725–4733.
- León, B., Ballesteros-Tato, A., Browning, J.L., Dunn, R., Randall, T.D., and Lund, F.E. (2012). Regulation of T(H)2 development by CXCR5+ dendritic cells and lymphotoxin-expressing B cells. *Nat. Immunol.* **13**, 681–690.
- Link, A., Vogt, T.K., Favre, S., Britschgi, M.R., Acha-Orbea, H., Hinz, B., Cyster, J.G., and Luther, S.A. (2007). Fibroblastic reticular cells in lymph nodes regulate the homeostasis of naive T cells. *Nat. Immunol.* **8**, 1255–1265.
- Lu, T.T., and Browning, J.L. (2014). Role of the lymphotoxin/LIGHT system in the development and maintenance of reticular networks and vasculature in lymphoid tissues. *Front. Immunol.* **5**, 47.
- Luther, S.A., Bidgol, A., Hargreaves, D.C., Schmidt, A., Xu, Y., Paniyadi, J., Matloubian, M., and Cyster, J.G. (2002). Differing activities of homeostatic chemokines CCL19, CCL21, and CXCL12 in lymphocyte and dendritic cell recruitment and lymphoid neogenesis. *J. Immunol.* **169**, 424–433.
- Massacand, J.C., Stettler, R.C., Meier, R., Humphreys, N.E., Grecis, R.K., Marsland, B.J., and Harris, N.L. (2009). Helminth products bypass the need for TSLP in Th2 immune responses by directly modulating dendritic cell function. *Proc. Natl. Acad. Sci. USA* **106**, 13968–13973.
- McCoy, K.D., Stoel, M., Stettler, R., Merky, P., Fink, K., Senn, B.M., Schaer, C., Massacand, J., Odermatt, B., Oettgen, H.C., et al. (2008). Polyclonal and specific antibodies mediate protective immunity against enteric helminth infection. *Cell Host Microbe* **4**, 362–373.
- Mionnet, C., Mondor, I., Jorquera, A., Loosveld, M., Maurizio, J., Arcangeli, M.-L., Ruddle, N.H., Nowak, J., Aurrand-Lions, M., Luche, H., and Bajénoff, M. (2013). Identification of a new stromal cell type involved in the regulation of inflamed B cell follicles. *PLoS Biol.* **11**, e1001672.
- Mohrs, M., Shinkai, K., Mohrs, K., and Locksley, R.M. (2001). Analysis of type 2 immunity in vivo with a bicistronic IL-4 reporter. *Immunity* **15**, 303–311.
- Morimoto, M., Morimoto, M., Whitmire, J., Xiao, S., Anthony, R.M., Mirakami, H., Star, R.A., Urban, J.F., Jr., and Gause, W.C. (2004). Peripheral CD4 T cells rapidly accumulate at the host: parasite interface during an inflammatory Th2 memory response. *J. Immunol.* **172**, 2424–2430.
- Mosconi, I., Dubey, L.K., Volpe, B., Esser-von Bieren, J., Zaiss, M.M., Lebon, L., Massacand, J.C., and Harris, N.L. (2015). Parasite proximity drives the expansion of regulatory T cells in Peyer's patches following intestinal helminth infection. *Infect. Immun.* **83**, 3657–3665.
- Mueller, S.N., and Germain, R.N. (2009). Stromal cell contributions to the homeostasis and functionality of the immune system. *Nat. Rev. Immunol.* **9**, 618–629.
- Mulu, A., Anagaw, B., Gelaw, A., Ota, F., Kassu, A., and Yifru, S. (2015). Effect of deworming on Th2 immune response during HIV-helminths co-infection. *J. Transl. Med.* **13**, 236.
- Roozendaal, R., and Mebius, R.E. (2011). Stromal cell-immune cell interactions. *Annu. Rev. Immunol.* **29**, 23–43.
- Roozendaal, R., Mempel, T.R., Pitcher, L.A., Gonzalez, S.F., Verschoor, A., Mebius, R.E., von Andrian, U.H., and Carroll, M.C. (2009). Conduits mediate transport of low-molecular-weight antigen to lymph node follicles. *Immunity* **30**, 264–276.
- Salgame, P., Yap, G.S., and Gause, W.C. (2013). Effect of helminth-induced immunity on infections with microbial pathogens. *Nat. Immunol.* **14**, 1118–1126.
- Schneider, K., Potter, K.G., and Ware, C.F. (2004). Lymphotoxin and LIGHT signaling pathways and target genes. *Immunol. Rev.* **202**, 49–66.
- Siegert, S., and Luther, S.A. (2012). Positive and negative regulation of T cell responses by fibroblastic reticular cells within paracortical regions of lymph nodes. *Front. Immunol.* **3**, 285.
- Sixt, M., Kanazawa, N., Selg, M., Samson, T., Roos, G., Reinhardt, D.P., Pabst, R., Lutz, M.B., and Sorokin, L. (2005). The conduit system transports soluble antigens from the afferent lymph to resident dendritic cells in the T cell area of the lymph node. *Immunity* **22**, 19–29.
- Urban, J.F., Jr., Noben-Trauth, N., Donaldson, D.D., Madden, K.B., Morris, S.C., Collins, M., and Finkelman, F.D. (1998). IL-13, IL-4R $\alpha$ , and Stat6 are required for the expulsion of the gastrointestinal nematode parasite *Nippostrongylus brasiliensis*. *Immunity* **8**, 255–264.
- Wang, X., Cho, B., Suzuki, K., Xu, Y., Green, J.A., An, J., and Cyster, J.G. (2011). Follicular dendritic cells help establish follicle identity and promote B cell retention in germinal centers. *J. Exp. Med.* **208**, 2497–2510.
- Wojciechowski, W., Harris, D.P., Sprague, F., Mousseau, B., Makris, M., Kusser, K., Honjo, T., Mohrs, K., Mohrs, M., Randall, T., and Lund, F.E. (2009). Cytokine-producing effector B cells regulate type 2 immunity to *H. polygyrus*. *Immunity* **30**, 421–433.
- Yang, C.-Y., Vogt, T.K., Favre, S., Scarpellino, L., Huang, H.-Y., Tacchini-Cottier, F., and Luther, S.A. (2014). Trapping of naive lymphocytes triggers rapid growth and remodeling of the fibroblast network in reactive murine lymph nodes. *Proc. Natl. Acad. Sci. USA* **111**, E109–E118.
- Zeng, M., Smith, A.J., Wietgreffe, S.W., Southern, P.J., Schacker, T.W., Reilly, C.S., Estes, J.D., Burton, G.F., Silvestri, G., Lifson, J.D., et al. (2011). Cumulative mechanisms of lymphoid tissue fibrosis and T cell depletion in HIV-1 and SIV infections. *J. Clin. Invest.* **121**, 998–1008.

**Cell Reports, Volume 15**

**Supplemental Information**

**Lymphotoxin-Dependent B Cell-FRC Crosstalk  
Promotes De Novo Follicle Formation and Antibody  
Production following Intestinal Helminth Infection**

**Lalit Kumar Dubey, Luc Lebon, Ilaria Mosconi, Chen-Ying Yang, Elke Scandella, Burkhard Ludewig, Sanjiv A. Luther, and Nicola L. Harris**

Figure S1 (Related to Figure 1)

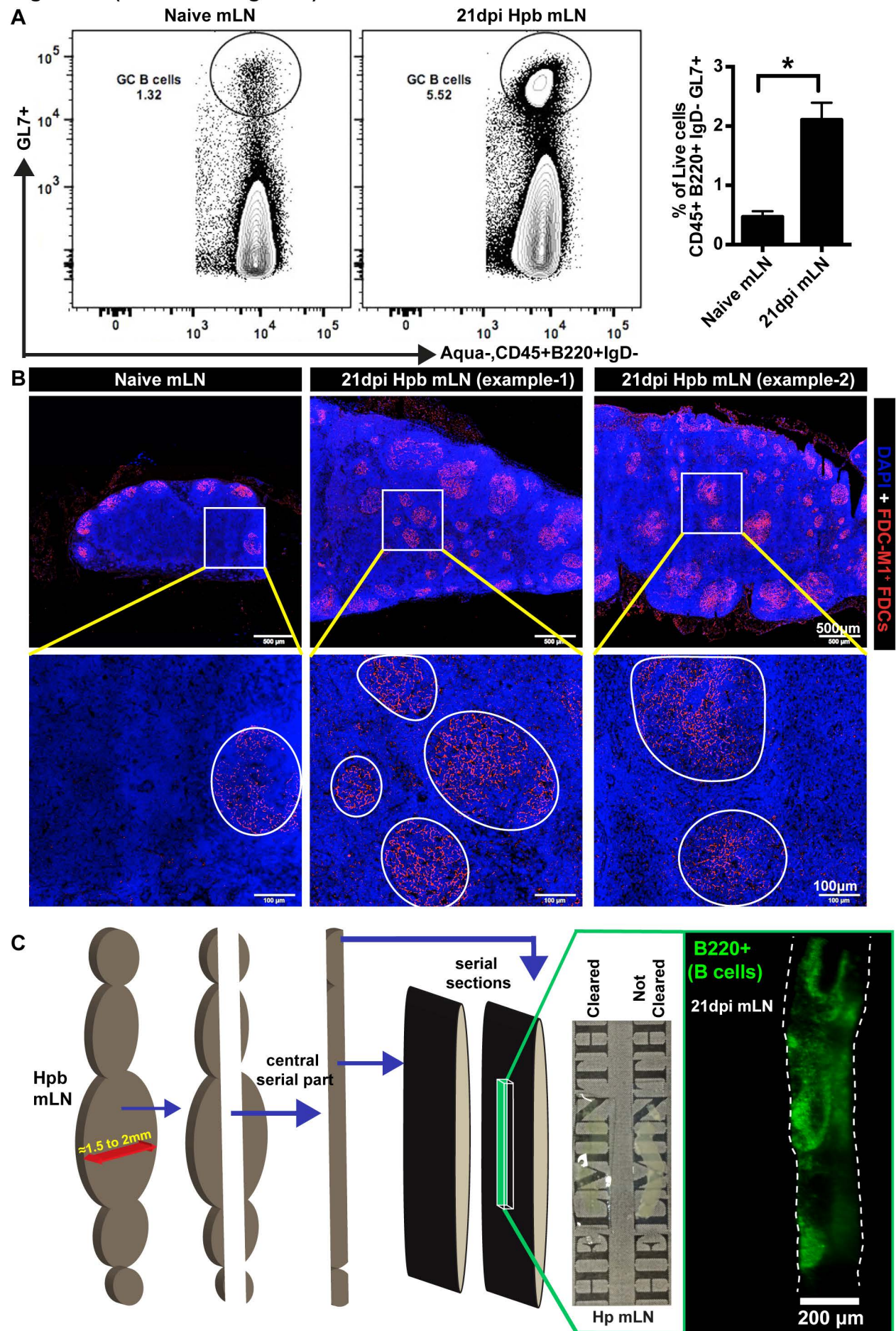


**Figure S1: *Hpb* infection triggers mLN swelling and *de novo* B cell follicle formation.**

(A) Representative dot plot FACS analysis with proportions of CD45<sup>+</sup>B220<sup>+</sup>IgD<sup>-</sup>GL7<sup>+</sup> germinal center (GC) B cells in the mLN of naïve and 21dpi *Hpb* infected C57BL/6J mice. The histogram represents pooled data from n≥3 mice. \**P* < 0.05, \*\**P* < 0.01, Mann-Whitney test. (B) Immunofluorescence images of the mLN follicular dendritic cell networks were defined using FDC-M1<sup>+</sup> (red) and DAPI (blue). Scale bar = 500µm and 100µm. (C) Pictorial representation of mLN showing vibratome sectioning which were used for clearing method. The right green panel shows the B220<sup>+</sup> B cell follicle distribution on a deep cleared mLN section.

Figure S2 (Related to Figure 2)

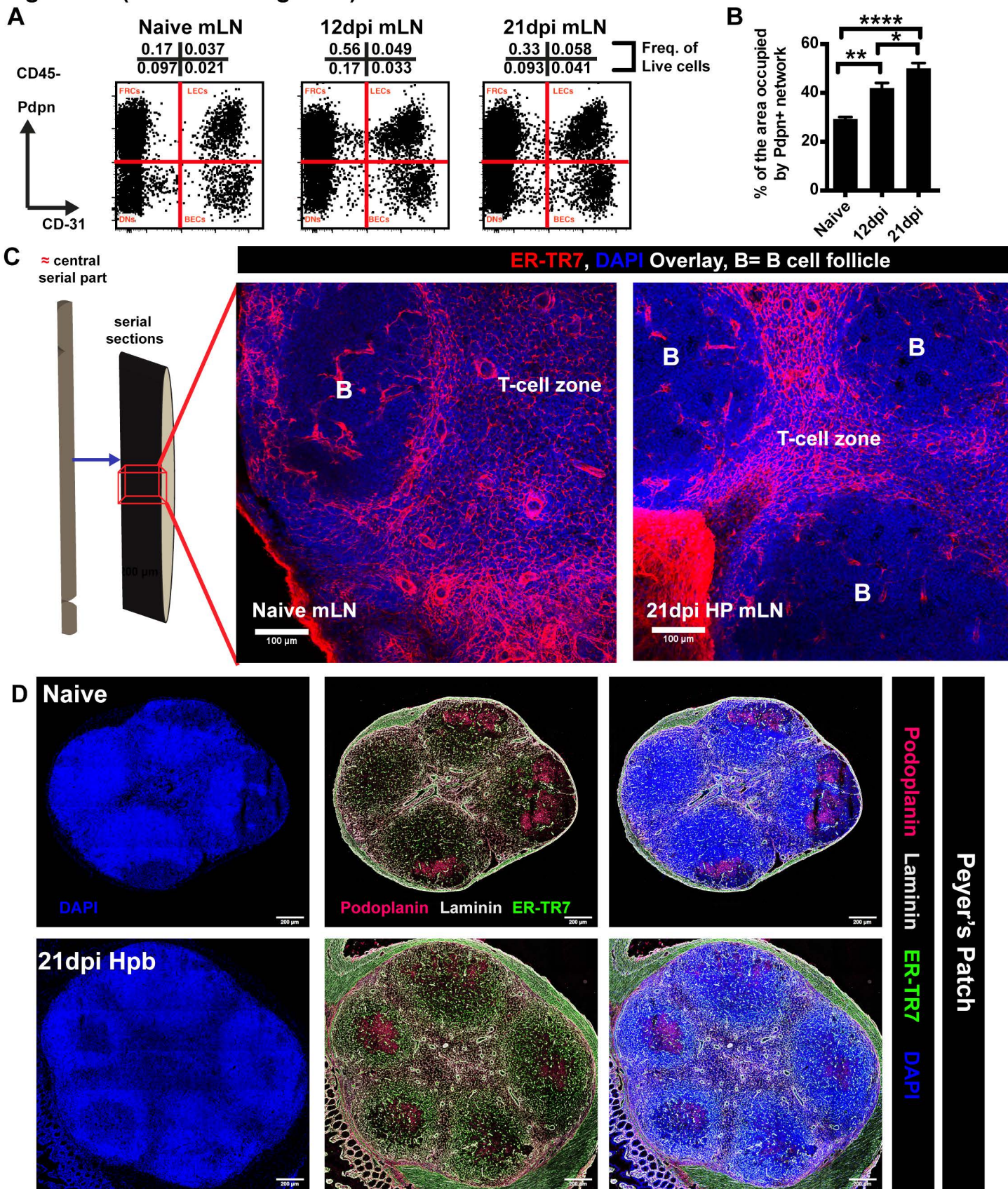


**Figure S2: *Hpb* infection promotes the expansion and re-organization of stromal cells in the mLN.**

(A) Representative dot plot analysis with values of FRCs, LECs, BECs and DN cells (pre-gated on live CD45<sup>+</sup> cells) showing the frequency of each stromal cell population. Each panel represents one individual mouse. (B) Immunofluorescence images were acquired and segmented using Image-J software and the number of pixels specific for Pdpn in the T cell zone determined and expressed as the percentage of total pixels in each area occupied by pdpn. Data represent mean  $\pm$  SEM (n = 4-6 images/mLN from 2 mice/time-point). (C) Immunofluorescence images of the mLN stromal reticular networks were defined using ERTR-7 (red) and DAPI (Blue). The detailed stromal reticular fibers are shown from the central section of mLN. Images are representative of two experiments with at least 2 mice/group/time points. Scale bar 100 $\mu$ m. (D) Immunofluorescence images of the Peyer's patch stromal reticular networks defined using ERTR-7 (green), Pdpn (red), Laminin (grey) and DAPI (blue). Scale bar 200 $\mu$ m.

Figure S3 (Related to Figure 3)

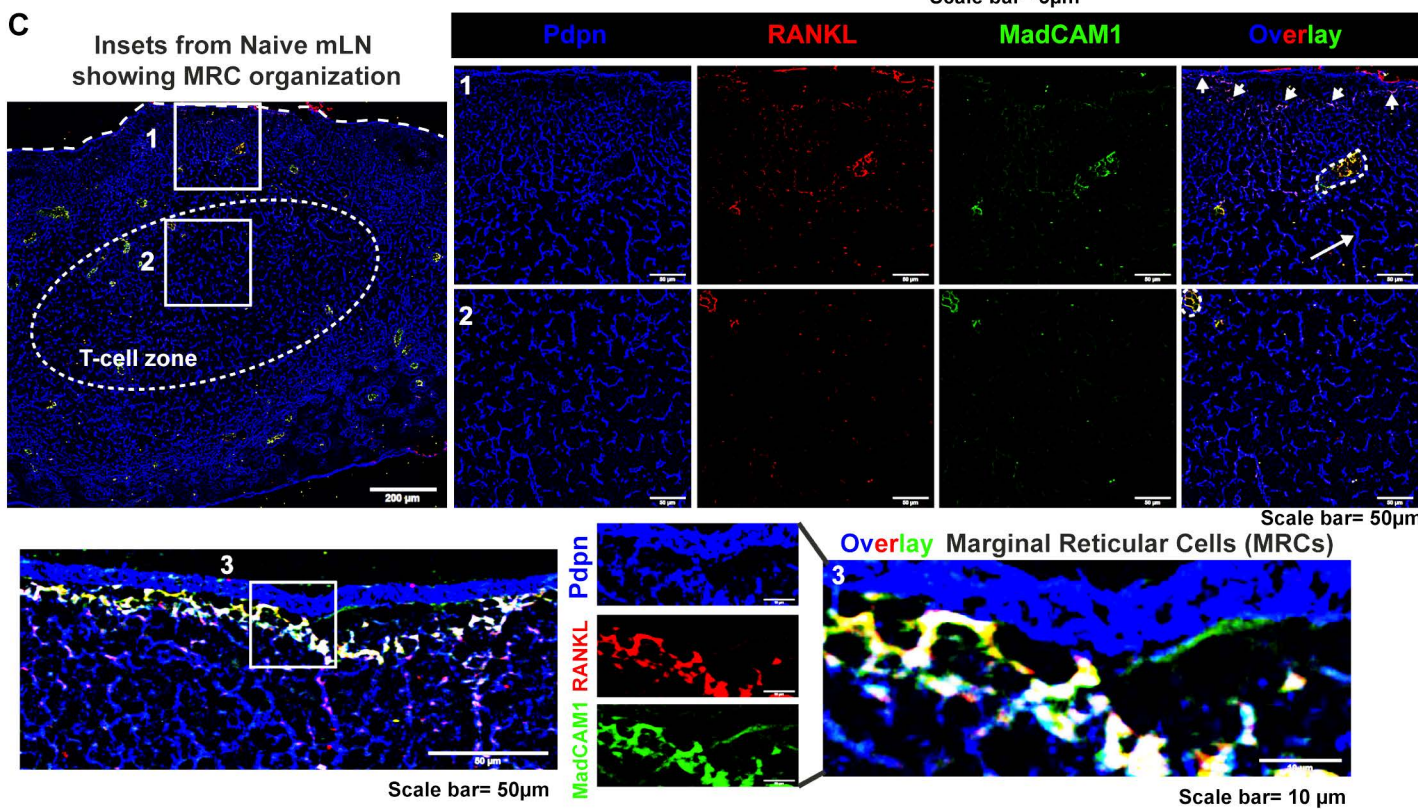
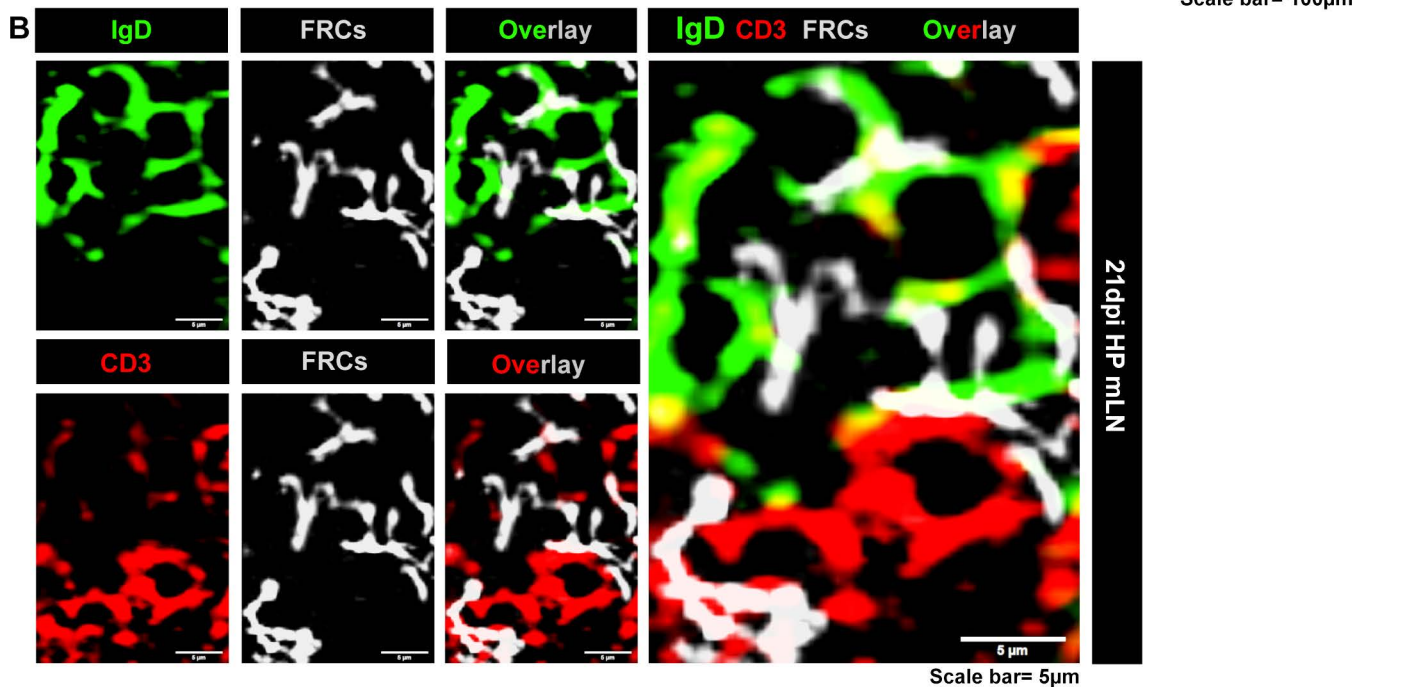
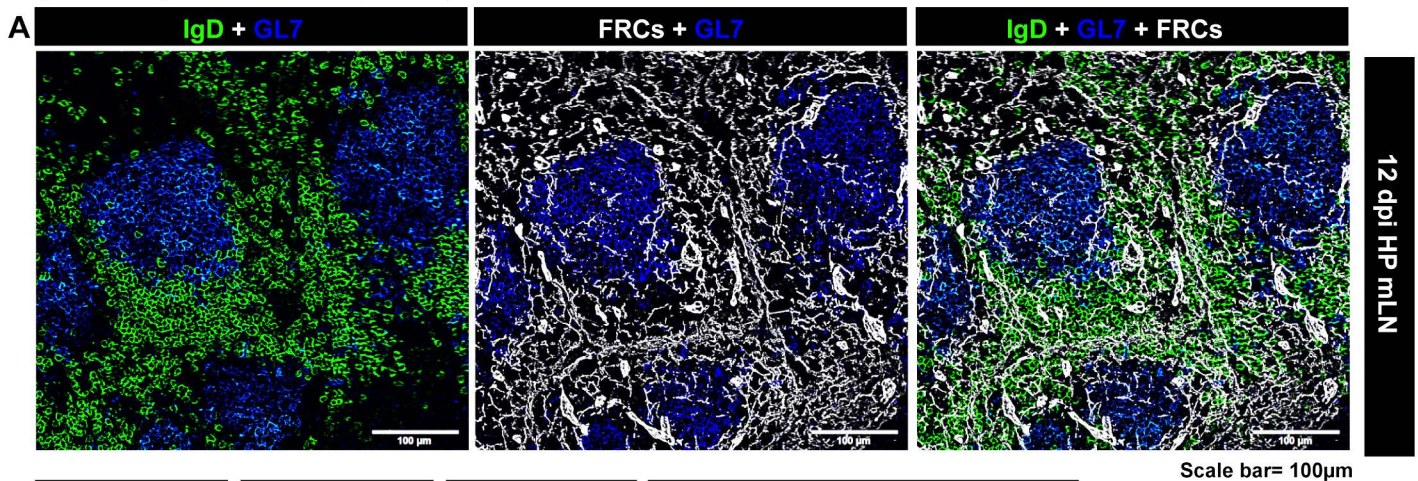


**Figure S3: FRCs provide a scaffold to B and T cells within the mantle of newly developed follicles that arise in response to *Hpb* infection.**

(A) Cryosections showing combined immunofluorescence images for naïve B cells (green; IgD<sup>+</sup>GL7<sup>-</sup>), T cells (red; CD3<sup>+</sup>), GC B cells (blue, IgD<sup>-</sup>GL7<sup>+</sup>) and FRC (white, IgD<sup>-</sup>GL7<sup>-</sup>CD3<sup>-</sup>Pdpn<sup>+</sup>Laminin<sup>+</sup>). Images are representative of mLN<sub>s</sub> collected from three independent experiments (n= 3 mice/time-point). (B) Higher magnification images showing single and combined staining for naïve B cells (green) and T cells (red) together with FRCs (white) as depicted in **Figure 3A-B**. Scale bar =5µm. (C) Naïve mLN showing single and combined immunofluorescence staining for marginal reticular cells (MRCs) identified as Pdpn<sup>+</sup>MadCAM1<sup>+</sup>RANKL<sup>+</sup>. Images are shown from the capsule edge (Box 1) as well as from the paracortical region (Box 2) of the mLN. A single layer of MRCs can be found below the subcapsular sinus (small arrow heads in Box 1, higher magnification view in Box 3), but these cells are absent in the central T cell zone under naïve settings (Box 2). The large arrow indicates T cell zone FRCs in the paracortical region.

Figure S4 (Related to Figure 4)

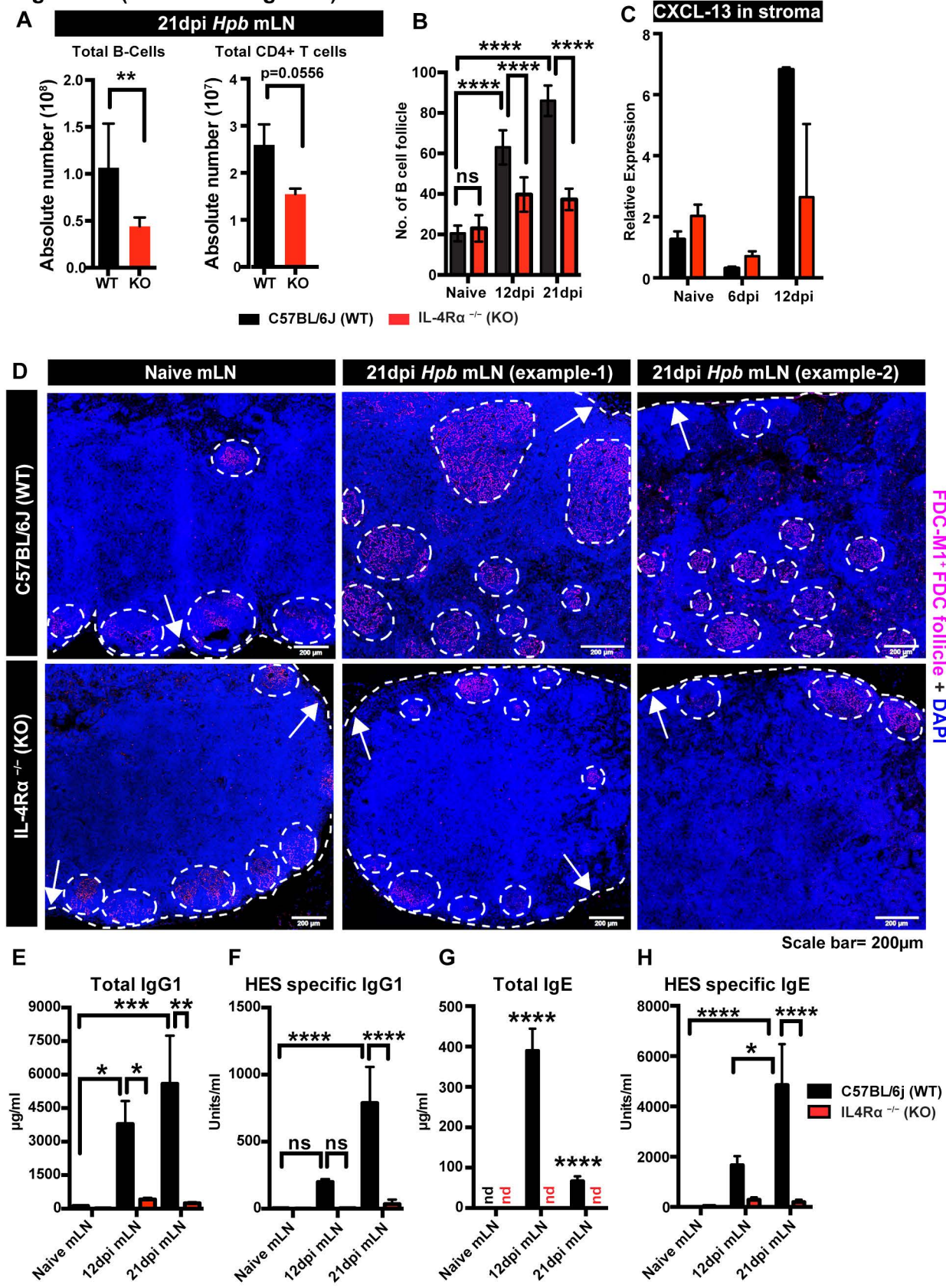


**Figure S4: mLN swelling and *de novo* B cell follicle formation in response to *Hpb* infection requires IL-4R $\alpha$  signaling.**

(A) Total number of B cells, and CD4<sup>+</sup> T cells in mLN of C57BL/6J (WT) and IL-4R $\alpha$ <sup>-/-</sup> (KO) mice as determined by flow cytometry. Data represent mean  $\pm$  SEM from one experiment and are representative of three independent experiments with n  $\geq$ 3-4 mice per group. (B) The number of B cell follicles (shown in Fig 4D) was counted on a graphic tablet at higher magnification (as described in Fig1). Data are presented as mean  $\pm$  SEM pooled from three independent experiments (n=2 mLN/group/time point). (C) CXCL13 expression in mLN stromal cells and (D) Immunofluorescence images showing FDC stromal networks identified using FDC-M1<sup>+</sup> cells (magenta) and nuclei counter-stained with DAPI (blue). White arrows indicate the capsule edge and white circles represent the FDC containing B cell follicles. Images are representative of three or more experiments with at least three mice/group/time point. Scale bar 200 $\mu$ m. (E-H) Serum antibody levels for (E) total IgG1, (F) HES specific IgG1, (G) total IgE and (H) HES specific IgE were determined by ELISA. Data is pooled from 2 independent experiments (n = 3–6 mice per group) and represents mean  $\pm$  SEM. nd; not detectable. \**P* < 0.05, \*\**P* < 0.01, \*\*\**P* < 0.001 and \*\*\*\**P* < 0.0001. (ANOVA, Bonferroni's multiple comparison test).

Figure S5 (Related to Figure 5)

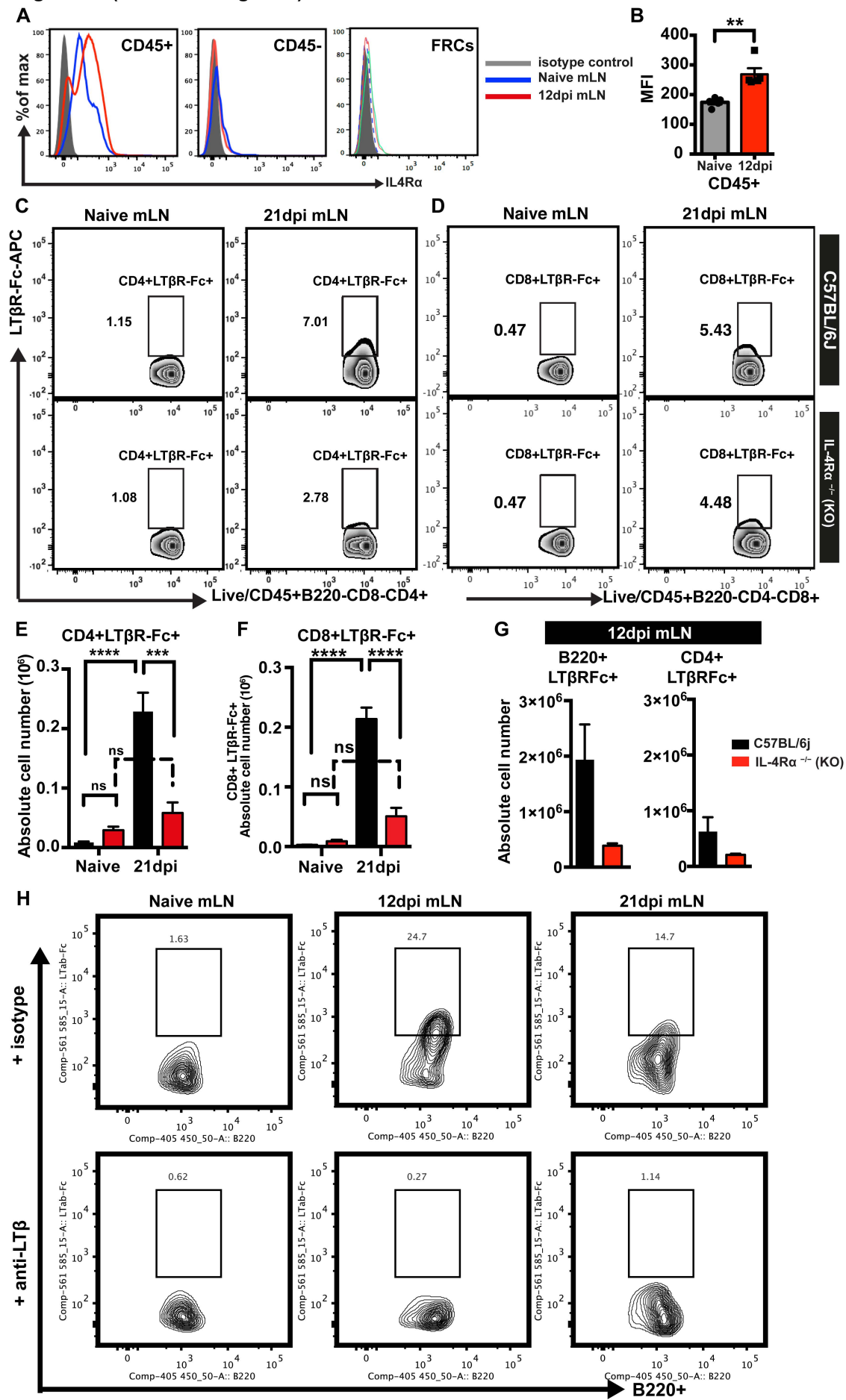


**Figure S5 (related to Figure 5): Stromal cell expansion and re-organization in response to *Hpb* infection requires IL-4R $\alpha$  signaling and lymphotoxin expression on lymphocytes.**

WT and IL-4R $\alpha$ <sup>-/-</sup> (KO) mice were infected with *Hpb* and the entire chain of the mLN collected at day 0 (naïve) and 12 dpi. Single cell suspensions were made and subjected to flow cytometric analysis of IL-4R $\alpha$  surface expression. **(A)** FACS histograms depicting IL-4R $\alpha$  expression by CD45<sup>+</sup>, CD45<sup>-</sup> and FRC cells. The majority of CD45<sup>+</sup> cells showed a substantial expression of IL-4R $\alpha$  whereas CD45<sup>-</sup> cells showed minimal to low expression and FRCs showed no detectable expression. **(B)** Bar graph of mean fluorescence intensity (MFI) of IL-4R $\alpha$  expression on CD45<sup>+</sup> cells. Data represent mean  $\pm$  SEM, of two independent experiments with n $\geq$ 3 mice/group/time points. \*\**P* < 0.01, (Mann-Whitney test). **(C-D)** Representative FACS plots showing CD4<sup>+</sup> and CD8<sup>+</sup> T cells positive for binding to LT $\beta$ R-Fc (pregated on live cells, which are CD45<sup>+</sup>B220<sup>-</sup>F4/80<sup>-</sup>FSH<sup>low</sup>). Each panel represents one individual mouse. **(E-F)** Total numbers of CD4<sup>+</sup> and CD8<sup>+</sup> T cells positive for LT $\beta$ R-Fc in mLN of C57BL/6J mice and IL-4R $\alpha$ <sup>-/-</sup> mice. Data are representative of 3 independent experiments (n = 3–4 mice per group/time point) and expressed as mean  $\pm$  SEM. **(G)** Total numbers of B cells and CD4<sup>+</sup> T cells positive for binding to LT $\beta$ R-Fc at 12 dpi. Data are representative of 3 independent experiments (n = 3–5 mice per group/time point) and expressed as mean  $\pm$  SEM. **(H)** FACS plots showing LT $\beta$ R-Fc binding of B cells from mLN of day 0, 12 and 21 dpi WT mice in the presence or absence of a blocking anti-LT $\beta$  mAb or isotype control. The absence of LT $\beta$ R-Fc binding by B cells in the presence of anti-LT $\beta$  indicates that these cells exclusively express the LT $\beta$ R ligand lymphotoxin but not LIGHT. Each panel represents one

individual mouse and is representative of 2 independent experiments (n = 3–5 mice per group/time point).

Figure S6 (Related to Figure 6)

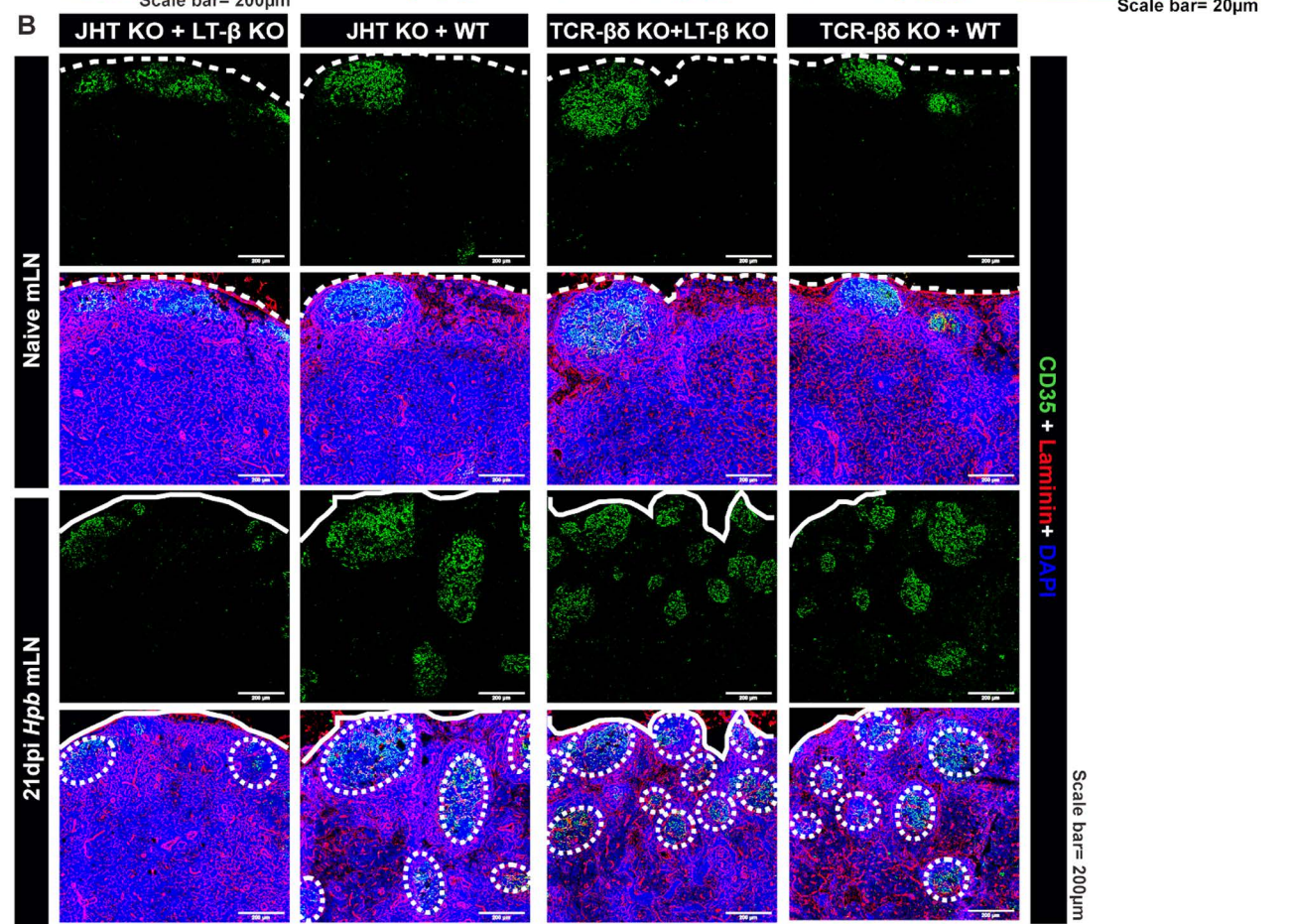
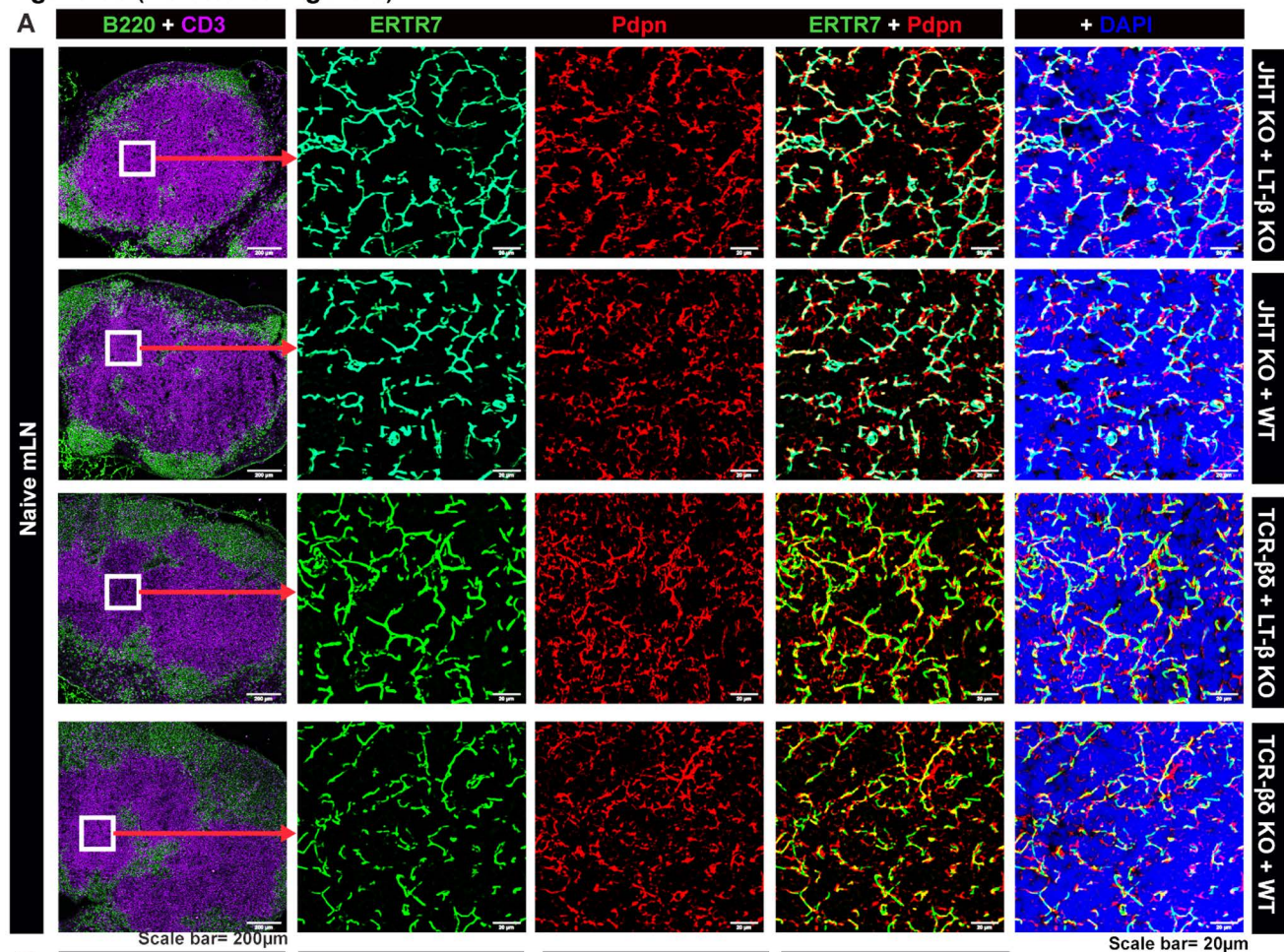


**Figure S6: Lymphotoxin producing B cells are required for *de novo* B cell follicle formation and T cell zone stromal cell expansion in response to *Hpb* infection.**

Mixed bone marrow chimeras were generated using lethally irradiated wildtype (WT) recipients reconstituted with bone marrow cells from B cell deficient ( $JHT^{-/-}$ ) or T cell deficient ( $TCR\beta\delta^{-/-}$ ) mice mixed with bone marrow cells from  $LT\beta^{-/-}$  mice at a 5:1 ratio. Resulting animals lacked lymphotoxin selectively on B cells ( $JHT^{-/-}$  +  $LT\beta^{-/-}$ ) or T cells ( $TCR\beta\delta^{-/-}$  +  $LT\beta^{-/-}$ ) and were compared to control mice receiving B or T cell deficient bone marrow mixed with WT cells ( $JHT^{-/-}$  + WT and  $TCR\beta\delta^{-/-}$  + WT). All mice were infected with *Hpb* and the entire chain of the mLN collected at day 0 (naïve) and 21 dpi. **(A)** Naïve mLN cryosections were stained for B cells (green,  $B220^{+}$ ), T cells (magenta,  $CD3^{+}$ ) or stromal cells (red,  $Pdpn^{+}$ ) (green,  $ERTR7^{+}$ ). Scale bars in  $B220^{+}CD3^{+}$  panel =200 $\mu$ m. Stromal cell staining representing the boxed areas shown in the B/T cell panel and highlighting  $Pdpn^{+}$  FRCs associated with  $ERTR7^{+}$  fibers. Scale bar =20 $\mu$ m. **(B)** Single and combined overlay immunofluorescence images of mLN cryosections showing FDCs (green,  $CD35^{+}$ ) and FRCs (red,  $laminin^{+}$ ) and nuclei (blue, DAPI). Mice lacking lymphotoxin on B cells failed to increase the number of FDC containing B cell follicles or to expand the stromal cell network. Scale bar =200 $\mu$ m.

Figure S7 (Related to Figure 7)

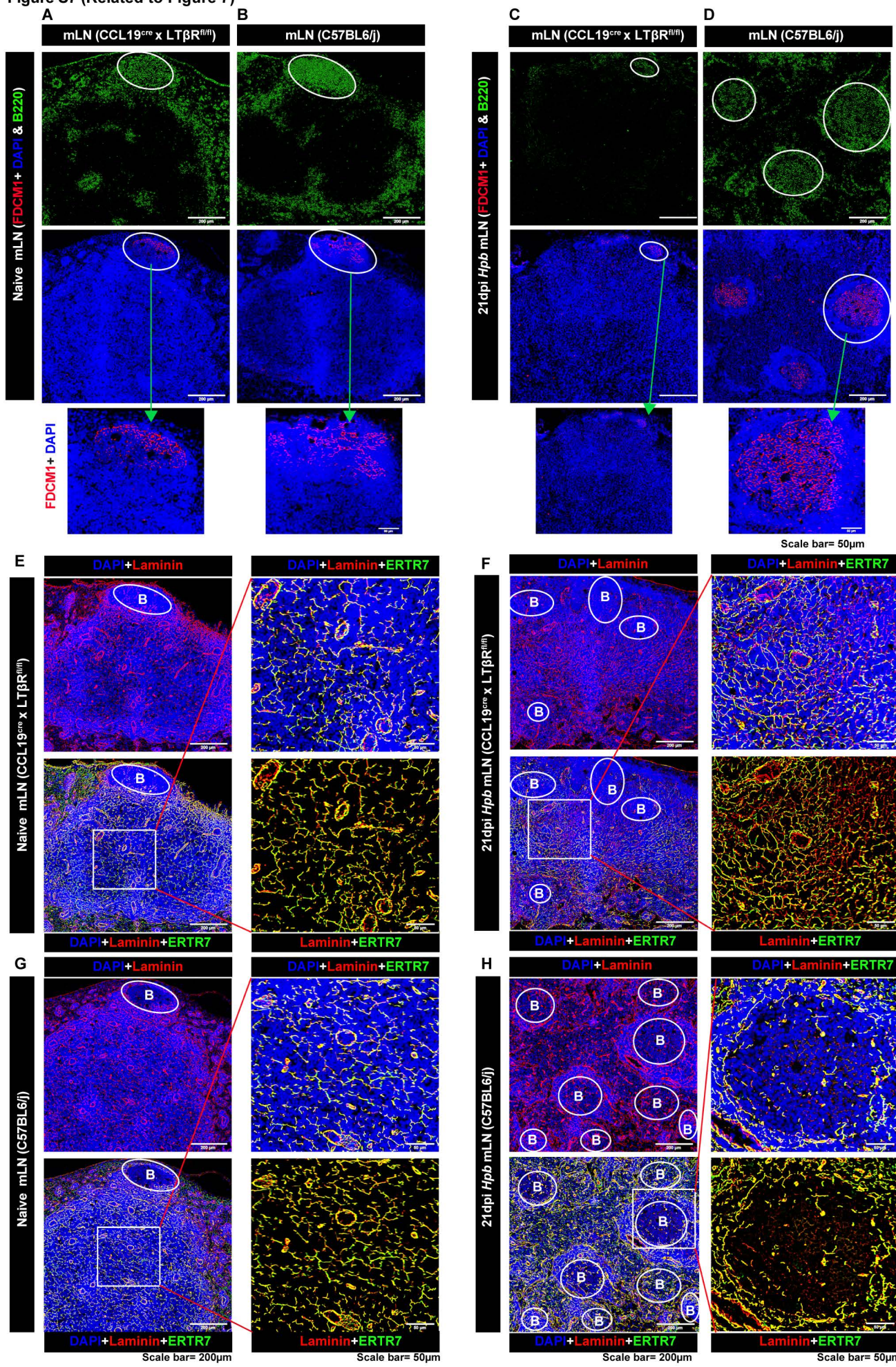


**Figure S7: LT $\beta$ R expression by CCL19<sup>-cre</sup> positive stromal cells is required for mLN swelling and stromal cell re-modeling in response to *Hpb* infection.**

CCL19<sup>-cre</sup> x LT $\beta$ R<sup>fl/fl</sup> and C57BL/6J mice were infected with *Hpb* and the entire chain of the mLN collected at day 0 (naïve) and 21 dpi. **(A-D)** Cryosections were stained for B cells (green, B220<sup>+</sup>), FDCs (red, FDCM1<sup>+</sup>) and nuclei (blue, DAPI). White circles indicate a B cell follicle and a higher magnification view of this area is shown. **(E-H)** Cryosections were stained for FRC associated matrix networks, as defined by laminin (red), and ERTR-7 (green) expression; nuclei were counterstained by DAPI (blue). Boxed areas within the deeper regions of the mLN are additionally shown at higher magnification. Images are representative of two independent experiments with at least two mice /group/ time-point. Scale bar 200 and 50  $\mu$ m.

**Related to Experimental procedure**

**Table-S1**

<b>S.No.</b>	<b>Target</b>	<b>Species</b>	<b>Clone</b>	<b>Conjugate</b>	<b>Catalogue No</b>	<b>Supplier</b>
1	a-LT $\beta$	Chimeric	Monoclonal	Purified	-----	Biogen Idec
2	B220	Rat	RA3-6B2	Pacific Blue	103227	Biologend
3	CD11c	Armenian Hamster	N418	APC	117310	Biologend
4	CD19	Rat	6D5	APC	115512	Biologend
5	CD3	Rat	17A2	Alexa 700	100216	Biologend
6	CD31	Rat	390	Pacific blue	102422	Biologend
7	CD32	Rat	390	PE	102408	Biologend
8	CD35	Rat	7E9	Alexa 488	123408	Biologend
9	CD4	Rat	RM4-5	PE	100512	Biologend
10	CD44	Rat	IM7	Alexa 700	103026	Biologend
11	CD45	Rat	30-F11	Alexa 488	103122	Biologend
12	CD45	Rat	30-F11	PEcy7	103114	Biologend
13	CD45	Rat	30-F11	Pacific Blue	103126	Biologend
14	CD62L	Rat	MEL14	BV605	104438	Biologend
15	CD8	Rat	YTS156.7.7	Alexa 488	126606	Biologend
16	F4/80	Rat	BM8	PerCP/cy5.5	123128	Biologend
17	GL7	Rat	GL7	Biotin	13-5902-85	eBiosciences
18	Human IgG	Goat	Polyclonal	Biotin	SAB3701279	Sigma Aldrich
19	IgD	Rat	11-26c.2a	Alexa 700	405730	Biologend
20	IL-4R $\alpha$	Rat	I015F8	PE	144804	Biologend
21	Isotype Ctr IgG	Rat	RTK2758	Alexa 488	400525	Biologend
22	Isotype Ctr IgG	Rat	RTK4530	Alexa 700	400628	Biologend
23	Isotype Ctr IgG	Rat	eBRG1	Biotin	13-4301	eBiosciences
24	Ki-67	Set	56/MOPC-2	PE	556027	BD Pharmingen
25	LTbR	Rat	eBio3C8 (3 $\mu$ )	biotin	13-5671-80	eBiosciences
26	LTbR	Rat	eBio3C8 (3 $\mu$ )	PE	12-5671-82	eBiosciences
27	LTbR-Fc	-----	recombinant	purified	-----	Biogen Idec
28	Lyve-1	Rat	Lyve-1	Alexa 488	FAB2125G	R&D systems
29	MadCAM-1	Rat	MECA-367	Alexa 488	120708	Biologend
30	MHC Class II	Rat	M5/114.15.2	Alexa 700	107622	Biologend
31	PDGFR $\alpha$ (CD140a)	Rat	APA5	biotin	13-1401-82	eBiosciences
32	PNA	lectin	lectin	Alexa 488	L21409	Invitrogen
33	Podoplanin	Syrian Hamster	8.1.1	Alexa 647	in house	Hybridoma
34	Podoplanin	Syrian Hamster	eBio8.1.1	eFluor 660	50-5381	eBiosciences
35	Streptavidin	-----	-----	PE	405204	Biologend
36	Streptavidin	-----	-----	APC	17-4317-82	eBiosciences
37	Ter119	Rat	TER-119	Alexa 488	116215	Biologend

**Related to Experimental procedure**

**Table-S2**

S.No.	Target	Species	Clone	Conjugate	Catalogue No	Supplier
<b>Primary Antibodies</b>						
1	B220	Rat	RA3-6B2	Biotin	RM2615	Life Technologies
2	B220	Rat	RA3-6B2	Purified	103202	BioLegend
3	CD3	Armenain hamster	145-2C11	Purified	100302	BioLegend
4	CD35	Rat	8C12	Purified	558768	BD Pharmingen
5	DAPI	-----	-----	Powder	D9542	Sigma-Aldrich
6	ER-TR7	Rat	ER-TR7	Purified	T-2109	BMA Biomedicals
7	FDCs	Rat	FDC-M1	Purified	551320	BD Pharmingen
8	MadCAM-1	Rat	MECA-367	Purified	120702	BioLegend
9	GL7	Rat	GL7	Biotin	13-5902-85	eBiosciences
10	Podoplanin (Pdpn)	Syrian Hamster	8.1.1	Purified	-----	Hybridoma
11	IgD	Rat	11-26c	Purified	1120-01	Southern Biotech
12	Laminin	Rabbit	----	Purified	L9393	Sigma-Aldrich
13	PDGFR $\alpha$	Rat	APA5	Biotin	13-1401-82	eBiosciences
14	PNA	-----	Lectin	Biotin	B-1075	Vector laboratories
15	RANKL (TRANCE)	Rat	IK22/5	Biotin	13-5952-82	eBiosciences
<b>Secondary Antibodies</b>						
1	Anti Armenian hamster	Goat	Polyclonal	Alexa 594	127-585-160	Jackson Immuno Research
2	Anti Armenian hamster	Goat	Polyclonal	Dylight 594	405504	Biolegend
3	Anti Rabbit IgG	Donkey	Polyclonal	Alexa 488	A21206	Molecular Probes
4	Anti Rabbit IgG	Donkey	Polyclonal	Alexa 568	A10042	Molecular Probes
5	Anti Rabbit IgG	Donkey	Polyclonal	Alexa 647	A31573	Invitrogen
6	Anti Rat IgG	Donkey	Polyclonal	Alexa 488	A21208	Molecular Probes
7	Anti Rat IgG	Goat	Polyclonal	Alexa 568	A11077	Molecular Probes
8	Anti Rat IgG	Donkey	Polyclonal	Biotin	712-065-153	Jackson Immuno Research
9	Anti Syrian hamster IgG	Goat	Polyclonal	Alexa 647	107-606-142	Jackson Immuno Research
10	Anti Syrian hamster IgG	Goat	Polyclonal	Alexa 488	107-545-142	Jackson Immuno Research
11	Streptavidin	----	----	Alexa 488	S-11223	Molecular Probes
12	Streptavidin	----	----	Alexa 568	S-11226	Molecular Probes
13	Streptavidin	----	----	Pacific blue	S-11222	Invitrogen
14	Streptavidin	----	----	Alexa 647	S-21374	Invitrogen